IEEE Access
Multidisciplinary | Rapid Review | Open Access Journal

Received April 7, 2021, accepted May 26, 2021, date of publication June 2, 2021, date of current version June 10, 2021.

Digital Object Identifier 10.1109/ACCESS.2021.3085515

Optimal Approximation of Fractional-Order Butterworth Filter Based on Weighted Sum of Classical Butterworth Filters

SHIBENDU MAHATA[1], NORBERT HERENCSAR[2], (Senior Member, IEEE), AND DAVID KUBANEK[2]

[1]Department of Instrumentation and Electronics Engineering, Dr. B. C. Roy Engineering College, Durgapur 713206, India
[2]Department of Telecommunications, Faculty of Electrical Engineering and Communication, Brno University of Technology, 61600 Brno, Czech Republic

Corresponding author: Norbert Herencsar (herencsn@ieee.org)

The research results described in this paper are supported by the Czech Science Foundation project No. 19-24585S.

ABSTRACT In this paper, a new two-steps design strategy is introduced for the optimal rational approximation of the fractional-order Butterworth filter. At first, the weighting factors of the summation between the n^{th}-order and the $(n+1)^{\text{th}}$-order Butterworth filters are optimally determined. Subsequently, this model is employed as an initial point for another optimization routine, which minimizes the magnitude-frequency error relative to the $(n+\alpha)^{\text{th}}$-order, where $\alpha \in (0, 1)$, Butterworth filter. The proposed approximant demonstrates improved performance about the magnitude mean squared error compared to the state-of-the-art design for six decades of bandwidth, but the introduced approach does not require a fractional-order transfer function model and the approximant of the s^{α} operator. The proposed strategy also avoids the use of the cascading technique to yield higher-order fractional-order Butterworth filter models. The performance of the proposed 1.5^{th}-order Butterworth filter in follow-the-leader feedback topology is verified through SPICE simulations and its hardware implementation based on Analog Devices AD844AN-type current feedback operational amplifier.

INDEX TERMS Analog filter approximation, approximation method, Butterworth filter, current feedback operational amplifier, fractional calculus, fractional-order filter, interpolation, low-pass filter, mean square error method, optimization method.

LIST OF ABBREVIATIONS

ARME	Absolute Relative Magnitude Error
CFE	Continued Fraction Expansion
CFOA	Current Feedback Operational Amplifier
CSA	Cuckoo Search Algorithm
EFADE	Enhanced Fitness Adaptive Differential Evolution
FC	Fractional Calculus
FOBF	Fractional-Order Butterworth Filter
FOTF	Fractional-Order Transfer Function
FO	Fractional-Order
IOTF	Integer-Order Transfer Function
ISA	Interior Search Algorithm
MARME	Maximum Absolute Relative Magnitude Error
MMSE	Maximum Mean Squared Error
MSE	Mean Squared Error
PSO	Particle Swarm Optimization
SD	Standard Deviation

LIST OF SYMBOLS

α	Fractional order
$C_{n+\alpha}$	Weighting factor
Δ_N	Hurwitz determinants
$D_{n+\alpha}$	Weighting factor
f_{min}	Fitness of initial point
Lb	Lower bound of design variables
L	Total number of sampled data points

The associate editor coordinating the review of this manuscript and approving it for publication was Shaoyong Zheng.

n	Order of classical Butterworth filter
R^2	Coefficient of Determination
s^α	Fractional-order Laplacian operator
ω_{max}	Upper bound of bandwidth
ω_{min}	Lower bound of bandwidth
ω_C	Cut-off frequency
ω	Angular frequency
X_P	Vector of design variables
X	Initial point vector
x_i	Coefficients of the proposed approximant

I. INTRODUCTION

In recent years, the theoretical concepts of fractional calculus (FC) have been exploited towards developing more accurate models of real-world systems [1]. The application of FC in filter theory has led to the generalization of the traditional integer-order filters to the fractional-order (FO) domain [2]. A FO filter achieves the non-integer order roll-off rate, which is not possible using the classical filters. FO filters find applications in biomedical signal processing (e.g., electrocardiogram and electroencephalograph processing), processing of music signals, etc. [3]–[5]. The generalized first-order [6], second-order [7], Butterworth [8], Chebyshev [9], [10], inverse-Chebyshev [11], elliptic [12], power-law [13], and double-exponent [14] filters have been reported in the literature. Various works have demonstrated the low-pass, high-pass, and band-pass filter characteristics based on the FO transfer function (FOTF) [15]–[18]. The implementation of FOTF models can be accomplished using fractance devices (also known as constant phase elements) [19]. The practical realization of fractors has drawn significant attention from researchers [3], [20]. Due to the unavailability of the fractance element as a commercial product, various emulation techniques to approximate the impedance characteristics of the fractor have been reported [21]–[24]. The FO Laplacian operator s^α, where $\alpha \in (0, 1)$, has been approximated using the integer-order transfer function (IOTF) based on several approaches [25]–[29]. Rational approximations of the FO generalized filters and systems were realized using optimization techniques [30], [31].

The FOTF models of the fractional-order Butterworth filter (FOBF) based on the s-plane to W-plane transformation technique were reported in [32]; however, the designs for irrational orders could not be generated. In [33], the $(1+\alpha)$-order Butterworth filter was approximated using three FOTF models by minimizing the magnitude-frequency error relative to a first-order low-pass Butterworth filter. Another recent work [34] applies the Particle Swarm Optimization (PSO) algorithm for the same purpose. Error minimization of FOTF models concerning the second-order Butterworth filter characteristics was reported using the Cuckoo Search Algorithm (CSA), Interior Search Algorithm (ISA), and speed-enhanced CSA-to-ISA [35]. High-pass and band-pass characteristics of the FOBF were achieved using several FOTF models reported in [36]. In [37], comparative studies were carried out for the Symbiotic Organisms Search algorithm optimized FOTF models to approximate the characteristics of the $(1+\alpha)^{\text{th}}$-order high-pass Butterworth filter.

A well-known method to transform the FOTF into an integer-order one is through the replacement of the operator s^α with its rational approximant in the FOTF model [34], [38]–[40]. For example, a third-order approximant was obtained in [34] by substituting s^α with the continued fraction expansion (CFE) based biquadratic model in the PSO-optimized FOTF. At the cost of additional hardware overhead, the bandwidth of the resultant IOTF can be increased by enhancing the order of the rational approximation of s^α. A recent work [41] reported that such an approximant, when treated as an initial point for a classical optimizer, that minimizes the modeling error about the ideal FOBF magnitude characteristic, can significantly enhance the design bandwidth. Gravitational Search and Powell's algorithms were employed in [42] and [43], respectively, to obtain the optimal third-order FOBF approximants. In [33], FOBF approximants of $(n+\alpha)^{\text{th}}$-order, where n is an integer, were obtained by cascading the $(1+\alpha)^{\text{th}}$-order model with the $(n-1)^{\text{th}}$-order Butterworth function. In [44], the optimal $(2+\alpha)^{\text{th}}$-order FOBF was designed by avoiding the cascading method. Optimal rational approximations of the band-pass Butterworth filter exhibiting the symmetric [45] and asymmetric [46] FO roll-off behavior were also reported. It may be noted that the definition of the FOBF is based on the magnitude function; their phase characteristic is not mathematically defined.

In this paper, a new two-steps optimal design technique for the rational approximation of the FOBF is introduced. The proposed method is based on the interpolation of n^{th} and $(n+1)^{\text{th}}$-order Butterworth filters to model the magnitude-frequency characteristic of the $(n+\alpha)^{\text{th}}$-order Butterworth filter optimally. Compared to the best performing method reported in the literature (the Constrained Optimization technique [41]), the proposed approach does not require a FOTF model and the approximant of the s^α operator. The suggested strategy also avoids the use of the cascading technique to yield higher-order FOBF models. The proposed models attain improved accuracy concerning the magnitude mean squared error (MSE) metric for six decades of bandwidth (0.001–1000 rad/s) when compared to the cited literature. A comparative study of the proposed method with the reported literature on the rational approximation of FOBFs is presented in Table 1. Discrete components based circuit implementation using the commercially available Analog Devices AD844AN-type current feedback operational amplifier (CFOA) is demonstrated to highlight the practical efficacy. Both SPICE simulations and experimental measurements reveal good agreement with the ideal FOBF magnitude characteristic.

The rest of the paper is structured as follows. In Section II, the proposed technique is introduced. MATLAB and SPICE simulations, along with hardware experimental results, are presented in Section III. Finally, the paper concludes in Section IV.

TABLE 1. Comparison between the rational approximation techniques for FOBF modeling. (NR: Not Reported).

Reference	[34]	[41]	[41]	[42]	[43]	[44]	Present Work
Method	Optimization and CFE- based substitution	Constrained Optimization	Pole-Zero Optimization	Unconstrained Optimization	Unconstrained Optimization	Constrained Optimization	Optimal Interpolation
FOTF Model	Required	Required	Not required	Not required	Not required	Not required	Not required
Approximant of s^{α}	Required	Required	Required	Not required	Not required	Not required	Not required
No. of design steps	2	2	2	1	2	1	2
Bandwidth (rad/s)	0.01–1.5	0.001–1000	0.001–1000	0.01–10	0.01–100	0.01–10	0.001–1000
Approximant order to model FOBF of order $(1+\alpha)$	3	3	3	3	3	5	3
Generalized expressions of $(1+\alpha)$-order model coefficients	Yes	Yes	NR	NR	NR	NR	Yes
Higher-order FOBFs through	NR	NR	NR	Cascading	Cascading	Optimization	Optimization
Stability achieved through	No constraints are needed	Routh's criteria	Bound values	Bound values determined using trial-and-error	No constraints are needed	Routh's criteria	Routh's criteria

II. PROPOSED TECHNIQUE

The theoretical magnitude-frequency response of a FOBF of order $(n+\alpha)$ is given by (1):

$$|B^{n+\alpha}(j\omega)| = \frac{1}{\sqrt{1+\left(\frac{\omega}{\omega_C}\right)^{2(n+\alpha)}}}, \tag{1}$$

where ω is the angular frequency and ω_C is the cut-off frequency expressed in radians per second (rad/s). The proposed design method comprises two steps, as detailed below.

A. STEP 1: OPTIMAL DETERMINATION OF WEIGHTING FACTORS

Consider the transfer function as defined by (2):

$$H^{n+\alpha}(s) = \frac{C_{n+\alpha}}{B_n(s)} + \frac{D_{n+\alpha}}{B_{n+1}(s)}, \tag{2}$$

where the weighting factors $C_{n+\alpha}$ and $D_{n+\alpha}$ are real and positive numbers; $B_n(s)$ and $B_{n+1}(s)$ are the classical Butterworth polynomials of order n and $n+1$, respectively.

In the first step, the optimal values of $C_{n+\alpha}$ and $D_{n+\alpha}$ are determined for a desired order of the normalized FOBF ($\omega_C = 1$ rad/s) by minimizing the cost function, as given by (3):

$$f = \frac{1}{L}\sum_{i=1}^{L} |20\log_{10}|B^{n+\alpha}(j\omega_i)| - 20\log_{10}|H^{n+\alpha}(j\omega_i, X)||^2, \tag{3}$$

where L denotes the total number of sampled frequency points with logarithmic spacing in the bandwidth $\omega \in [\omega_{min}, \omega_{max}]$ rad/s; and $X = [C_{n+\alpha}\ D_{n+\alpha}]$ is the vector of design variables.

After the optimization procedure, $H^{n+\alpha}(s)$ may be represented as per (4):

$$H^{n+\alpha}(s) = \frac{u_1 s^{n+1} + u_2 s^n + \cdots + u_{n+2}}{s^{2n+1} + u_{n+3}s^{2n} + u_{n+4}s^{2n-1} + \cdots + u_{3n+3}}, \tag{4}$$

where the coefficients of $H^{n+\alpha}(s)$ are given by u_i ($i = 1, 2, \ldots, 3n+3$).

B. STEP 2: OPTIMAL DETERMINATION OF COEFFICIENTS FOR THE FOBF APPROXIMANT

The proposed FOBF approximant is modeled as per (5):

$$T^{n+\alpha}(s) = \frac{P(s)}{Q(s)} = \frac{x_1 s^{n+1} + x_2 s^n + \cdots + x_{n+2}}{s^{2n+1} + x_{n+3}s^{2n} + x_{n+4}s^{2n-1} + \cdots + x_{3n+3}}, \tag{5}$$

where the coefficients of $T^{n+\alpha}(s)$ are denoted by x_i ($i = 1, 2, \ldots, 3n+3$).

The coefficients of $H^{n+\alpha}(s)$, i.e., u_i ($i = 1, 2, \ldots, 3n+3$), are treated as an initial point for the second minimization routine, whose fitness function (MSE) is given by (6), to determine the optimal values of the coefficients of $T^{n+\alpha}(s)$:

$$MSE = \frac{1}{L}\sum_{i=1}^{L} |20\log_{10}|B^{n+\alpha}(j\omega_i)| - 20\log_{10}|T^{n+\alpha}(j\omega_i, X_P)||^2, \tag{6}$$

where $X_P = [x_1\ x_2\ \ldots\ x_{3n+3}]$ represents the vector of design variables comprising the coefficients of $T^{n+\alpha}(s)$.

To guarantee the generation of stable approximants, the inequality constraints as given by (7), are incorporated in the optimization routine:

$$\Delta_1, \Delta_2, \Delta_3, \cdots, \Delta_N > 0\ (N = 2n+1), \tag{7}$$

where,

$$\Delta_1 = d_{N-1},$$

$$\Delta_2 = \begin{vmatrix} d_{N-1} & d_{N-3} \\ d_N & d_{N-2} \end{vmatrix}, \quad \Delta_3 = \begin{vmatrix} d_{N-1} & d_{N-3} & d_{N-5} \\ d_N & d_{N-2} & d_{N-4} \\ 0 & d_{N-1} & d_{N-3} \end{vmatrix},$$

$$\ldots, \quad \Delta_N = \begin{vmatrix} d_{N-1} & d_{N-3} & d_{N-5} & \cdots & 0 \\ d_N & d_{N-2} & d_{N-4} & \cdots & 0 \\ 0 & d_{N-1} & d_{N-3} & \cdots & 0 \\ \vdots & \vdots & \vdots & \vdots & \vdots \\ 0 & 0 & 0 & \cdots & d_0 \end{vmatrix}$$

are the Hurwitz determinants [47]; and $Q(s) = \sum_{k=0}^{N} d_k s^k$.

The pseudocode of the proposed FOBF design technique is presented in Algorithm 1.

Algorithm 1: Pseudocode of the Proposed Optimal FOBF Modeling Technique

Inputs : n, α
Outputs: X, X_P

begin
  Set $\omega_{\min}$, $\omega_{\max}$, L, lower bound (Lb) for X and X_P
  for $k = 1$ **to** 100 **do**
    x_0 (Initial point of X) $\leftarrow$ $rand(0, 1)$
    Minimize (3)
    Store f_k and X_k
  $f_{\min} \leftarrow \min\{f_k\}$
  $X \leftarrow X_k$ corresponding to $f_{\min}$
  Calculate u_i $(i = 1, 2, \ldots, 3n + 3)$
  Minimize (6) and display X_P

III. SIMULATION RESULTS, EXPERIMENTAL VERIFICATION, AND DISCUSSIONS

The cost functions (3) and (6) are minimized using the MATLAB programming language (software version: MATLAB 2014a) with function *fmincon* (algorithm: '*active-set*') based on the following parameter settings: *MaxFunEvals* = 50000, *MaxIter* = 5000, *TolFun* = 1E–10, and *TolX* = 1E–10. The lower bound (Lb) for X is set as 0. The initial point (x_0) for X to minimize (3) is a randomly chosen value (drawn from uniform distribution) between 0 and 1. Hundred independent trial runs of the algorithm are carried out for Step 1. The optimal value of X, which achieves the minimum value of f, (i.e., f_{min}) is identified as the best solution from Step 1. The Lb of the design variables for the optimization procedure in Step 2 is chosen as 1E–8. The value of L is set as 1000.

A. DESIGN OF FOBFs FOR n = 1

This section deals with the performance assessment of the proposed technique for the design of FOBFs with $n = 1$.

1) CHOICE OF THE WEIGHTING FACTORS

Two different choices for the weighting factors may be considered as follows:

Case 1: $C_{1+\alpha}$ and $D_{1+\alpha}$ are determined by fixing their upper bound (Ub) as 2.

Case 2: A special case arises from the previous one when $D_{1+\alpha} = 1 - C_{1+\alpha}$. For this condition, a single variable minimization can be carried out instead of the two-variable one for Case 1. The Ub for $C_{1+\alpha}$ is set as 1.

The optimal values of $C_{1+\alpha}$ and $D_{1+\alpha}$ (Case 1) with α varying from 0.01 to 0.99 in steps of 0.01, are plotted in Figure 1 (*top left*). It is found that (i) $C_{1+\alpha}$ reduces from 0.9635 for $\alpha = 0.01$ and monotonically decreases to 0 as α increases; and (ii) $C_{1+\alpha}$ becomes exactly 0 for $\alpha = 0.99$. In the case of $D_{1+\alpha}$, it is found that (i) the value increases from 0.03771 at $\alpha = 0.01$, crosses one at $\alpha = 0.43$, yields a peak of 1.208 for $\alpha = 0.71$–0.74, and then decreases towards 1 (precisely attaining 1.017 at $\alpha = 0.99$); and (ii) unlike the plot for $C_{1+\alpha}$, slight abruptness in the value of $D_{1+\alpha}$ is noticed at $\alpha = 0.90, 0.92, 0.93$, and 0.94. The overall trend for $C_{1+\alpha}$ and $D_{1+\alpha}$ concurs with the fact that for lower (higher) values of α, the first-order (second-order) Butterworth filter responses play a dominant role in shaping the magnitude-frequency behavior of the FOBF.

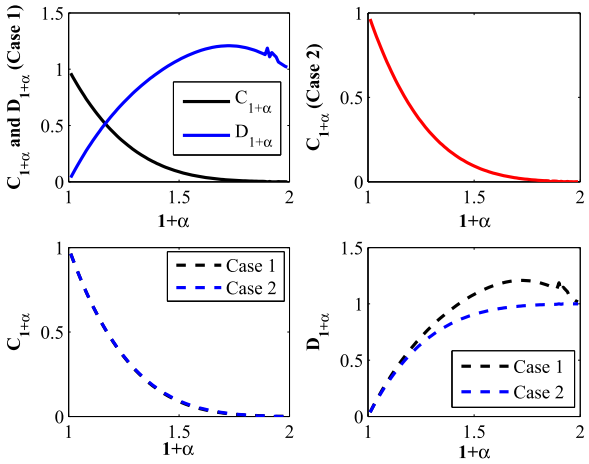

FIGURE 1. Optimal values of $C_{1+\alpha}$ and $D_{1+\alpha}$.

The optimal values of $C_{1+\alpha}$ (Case 2), as plotted in Figure 1 (*top right*), show a monotonically decreasing character with increasing α. Comparison of $C_{1+\alpha}$ obtained for Cases 1 and 2, as illustrated in Figure 1 (*bottom left*), reveals almost identical curves. The coefficient of determination (R^2) for $C_{1+\alpha}$ based on these two cases is 0.999949, which confirms a close matching.

Comparisons about $D_{1+\alpha}$ for the two cases are presented in Figure 1 (*bottom right*). It is observed that (i) the two plots are nearly the same up to $\alpha = 0.11$; (ii) for $\alpha > 0.11$, $D_{1+\alpha}$ acquires a higher value for Case 1 when compared to Case 2. This is possible due to the choice of the

TABLE 2. Optimal coefficients of the proposed FOBF approximants.

Case	α	x_1	x_2	x_3	x_4	x_5	x_6
1	0.20	0.27028	55.94965	497.84005	112.42937	631.72419	493.986520
	0.50	0.03542	12.69913	167.32240	70.777280	236.11550	165.25241
	0.80	0.00352	2.848450	58.483290	43.802790	85.220370	58.023920
	0.86	0.00201	2.097090	47.524830	39.544840	69.208810	47.246630
2	0.20	0.27028	55.94965	497.84791	112.42975	631.73361	493.99479
	0.50	0.03542	12.69913	167.32059	70.776840	236.11321	165.25061
	0.80	0.00352	2.848450	58.483560	43.802870	85.220730	58.024160
	0.86	0.00201	2.097090	47.524080	39.544340	69.207770	47.245900

higher value of Ub ($=2$) for $D_{1+\alpha}$ with Case 1. It may be recalled that the roll-off rate for a 1.5$^{\text{th}}$-order FOBF (–30 dB/decade) lies exactly in-between that of the first-order and second-order Butterworth filters. However, the values of $C_{1+\alpha}$ and $D_{1+\alpha}$ for Case 2 at $\alpha = 0.5$ are 0.09374 and 0.90626, respectively. These values of weighting factors highlight that the second-order Butterworth response is more dominant in characterizing the behavior of the 1.5$^{\text{th}}$-order model based on the optimization procedure proposed in Step 1.

A comparison of the cost function value (f) for Cases 1 and 2 is presented in Figure 2. It is found that both cases attain a similar fitness for $\alpha \leq 0.26$. With a further increase in the design order, the error achieved by Case 1 is lower than Case 2. Thus, a better accuracy may be achieved in Step 1 of the proposed method by allowing independent variations of the weighting factors. It may be noted that abruptly high value of f is observed for $\alpha = \{0.90, 0.92\}$ and $\alpha = \{0.86, 0.90, 0.92, 0.95\}$ for Cases 1 and 2, respectively.

The MSE achieved by the proposed FOBF approximants for $\alpha \in (0.01, 0.99)$ based on Cases 1 and 2 is compared in Figure 3. It is found that a spike in the fitness value is yielded at $\alpha = \{0.02, 0.05, 0.06\}$ and $\alpha = 0.05$ for Cases 1 and 2, respectively. For all other orders, the same value of MSE is achieved for both cases. It is worth emphasizing that although Case 1 produces a better fitness for $\alpha > 0.26$ after Step 1, and hence, a better initial point, however, the final solution quality of the FOBF approximant (obtained after Step 2) for these orders remains the same for both cases. Therefore, Case 2 may be preferred over Case 1 since Case 2 requires only one design variable.

For Case 1, the optimal values of $[\, C_{1+\alpha}\ D_{1+\alpha}\,]$ with $\alpha = 0.2, 0.5, 0.8,$ and 0.86, are $[\,0.4452\ 0.5973\,]$, $[\,0.08886\ 1.084\,]$, $[\,0.008148\ 1.192\,]$, and $[\,0.004407\ 1.155\,]$, respectively. The optimal values of $C_{1+\alpha}$ for Case 2 with $\alpha = \{0.2, 0.5, 0.8, 0.86\}$ are {0.4474, 0.09374, 0.009298, 5.551E–17}. Since $C_{1+\alpha}$ is practically zero for Case 2 with $\alpha = 0.86$, therefore, the corresponding initial point exhibits the behavior of a second-order Butterworth filter. This finding explains the appreciably large f yielded for $\alpha = 0.86$ in Case 2 (see Figure 2). The optimal values of coefficients of the proposed FOBFs for various values of α obtained for Cases 1 and 2 are presented in Table 2. The similarity of the model coefficients

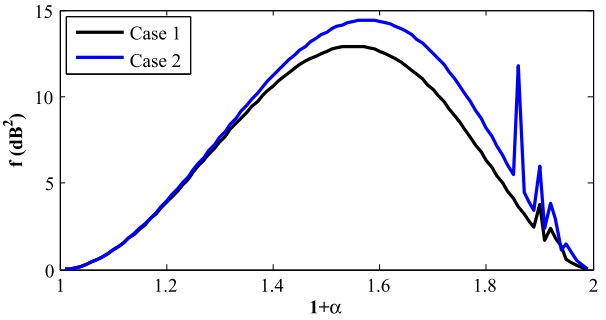

FIGURE 2. Comparison between the fitness values (f) achieved for Case 1 and Case 2.

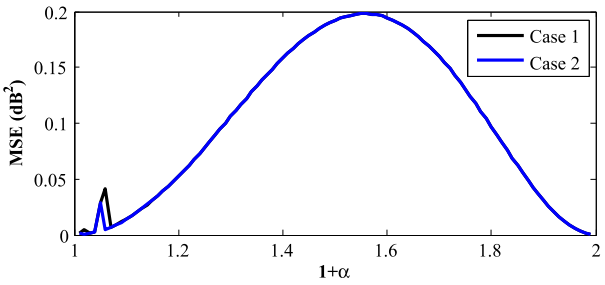

FIGURE 3. Comparison between the MSE values achieved for Case 1 and Case 2.

obtained for both cases may explain the resemblance of the error curves presented in Figure 3.

Figures 4(a)–(d) show the magnitude-frequency plots of the approximants obtained after Step 1 (*top*) and Step 2 (*bottom*) for $\alpha = 0.2, 0.5, 0.8,$ and 0.86, respectively. For all the four considered cases, it is observed that the responses of the initial point (top sub-plot in Figure 4) substantially depart from the ideal behavior. These responses are based on the transfer function (2), which is an intermediate step in the proposed FO filter design method and is not used for the filter circuit implementation. It is only an initial point for the Step 2, which leads to the transfer function (5), as illustrated by the bottom responses in Figure 4. Thus, the final design obtained after Step 2 can approximate the ideal characteristic (1) with much better accuracy. That is, the proposed FOBF (obtained after Step 2) exhibits good agreement with the theoretical characteristics. It may be noted from Figure 4(d) that the magnitude plots of the initial point based on Case 1 is closer to the ideal one in comparison to that attained for

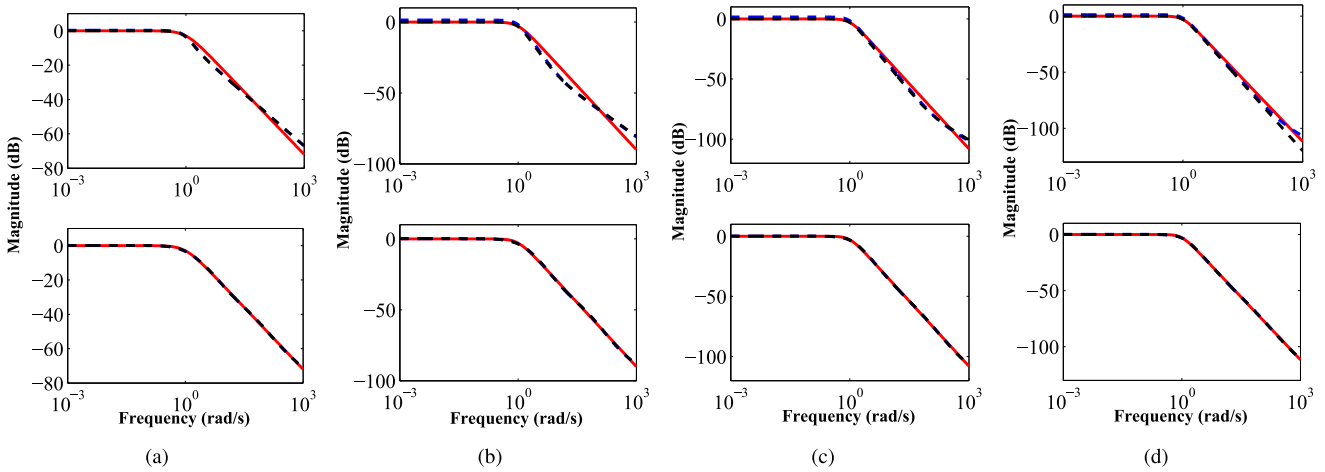

FIGURE 4. Magnitude-frequency comparison plots of the approximants based on Case 1 (*dashed blue*), Case 2 (*dashed black*), and the ideal FOBF (*solid red*) after Step 1 (*top*) and Step 2 (*bottom*) for (a) $\alpha = 0.2$, (b) $\alpha = 0.5$, (c) $\alpha = 0.8$, and (d) $\alpha = 0.86$.

TABLE 3. Constraints incorporated with the cost function given in (6).

Case	Constraints incorporated to ensure	Constraints for the design of $(1+\alpha)$-order FOBF
1	Design Stability	$x_6 - x_4x_5 < 0$
2	(i) Design Stability	(i) $x_6 - x_4x_5 < 0$
	(ii) $\left\|T^{n+\alpha}(j1)\right\| = \frac{1}{\sqrt{2}}$	(ii) $\frac{\sqrt{(x_3-x_1)^2+(x_2)^2}}{\sqrt{(x_6-x_4)^2+(x_5-1)^2}} = \frac{1}{\sqrt{2}}$
3	(i) Design Stability	(i) $x_6 - x_4x_5 < 0$
	(ii) $\left\|T^{n+\alpha}(j0)\right\| = 1$	(ii) $x_6 = x_3$
4	(i) Design Stability	(i) $x_6 - x_4x_5 < 0$
	(ii) $\left\|T^{n+\alpha}(j1)\right\| = \frac{1}{\sqrt{2}}$	(ii) $\frac{\sqrt{(x_3-x_1)^2+(x_2)^2}}{\sqrt{(x_6-x_4)^2+(x_5-1)^2}} = \frac{1}{\sqrt{2}}$
	(iii) $\left\|T^{n+\alpha}(j0)\right\| = 1$	(iii) $x_6 = x_3$

TABLE 4. Comparison between the designed FOBFs ($n = 1$) for $\alpha = 0.46$ and 0.68.

α	Case	$C_{1+\alpha}$	f (dB^2)	MSE (dB^2)	X_P	$\left\|T^{1+\alpha}(j0)\right\|$ (dB)	$\left\|T^{1+\alpha}(j1)\right\|$ (dB)
0.46	1	0.1193	12.9141	0.1819	[0.0469 15.4652 192.9846 75.2824 269.6583 190.6172]	0.107	–3.622
	2	0.1193	12.9141	2.6445	[0.0713 4.8525 1E–8 5.8213 4.6354 1E–8]	–3.654	–3.010
0.68	1	0.0266	13.0863	0.1694	[0.0094 5.2078 88.7566 53.3394 128.7260 87.7992]	0.094	–3.495
	2	0.0266	13.0863	2.5042	[0.0151 2.6980 1E–8 3.4686 2.5922 0.0011]	–100.7	–3.010

Case 2. This confirms the lower value of f achieved for Case 1 (3.654 dB^2) than Case 2 (11.780 dB^2) at $\alpha = 0.86$.

2) INCORPORATION OF ADDITIONAL CONSTRAINTS

From (1), it follows that a normalized FOBF exhibits: (i) $\left|B^{n+\alpha}(j0)\right| = 1$, and (ii) $\left|B^{n+\alpha}(j1)\right| = \frac{1}{\sqrt{2}}$. The strategy proposed in Section II guarantees the generation of stable approximants only; no specific constraints were incorporated to satisfy the ideal magnitude responses at 0 and 1 rad/s. In this sub-section, comparative studies are conducted by introducing additional constraints in the proposed optimization technique to achieve the two aforementioned characteristics. For this purpose, Table 3 presents four design cases based on the constraints incorporated to minimize (6), with Step 1 modeled by $D_{1+\alpha} = 1 - C_{1+\alpha}$.

The magnitude values of the designed $(1+\alpha)$-order FOBFs for $\omega = 0$ rad/s based on the four cases are presented in Figure 5. It is observed that Case 1 (*top left*) and Case 2 (*top right*) exhibit the worst response, which is expected since no explicit constraints are incorporated to ensure that the magnitude of the approximant at $\omega = 0$ rad/s satisfies the ideal value of 0 dB.

For Case 1, the largest deviation occurs for $\alpha = 0.01$, where a magnitude of –0.6055 dB at 0 rad/s is obtained. For the same order, Case 2 yields a magnitude of 0.0034 dB. Except for $\alpha = 0.46$ and 0.68, $\left|T^{1+\alpha}(j0)\right|$ for the designs based on Cases 1 and 2 for all the other orders are similar (*middle*). For Case 3 (*bottom left*) and Case 4 (*bottom right*), including the equality constraint $x_6 = x_3$ ensures that $\left|T^{1+\alpha}(j0)\right| \approx 0$ dB for all the considered values of α.

The discrepancies in the magnitude at 0 rad/s of the FOBFs based on Cases 1 and 2 at $\alpha = 0.46$ and 0.68 are investigated by tabulating the performance metrics and design variables

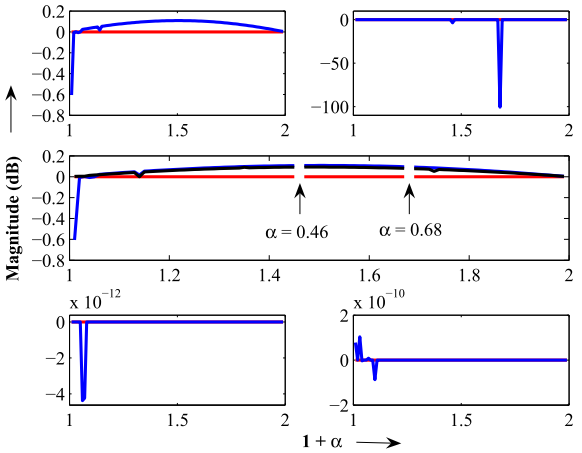

FIGURE 5. Magnitude (dB) at DC (i.e., $\omega = 0$ rad/s) for the ideal (*red*) and the designed FOBFs (*blue*) based on Case 1 (*top left*), Case 2 (*top right*), Case 3 (*bottom left*), and Case 4 (*bottom right*). Figure in the *middle* shows the comparison plots between Case 1 (*blue*) and Case 2 (*black*) based FOBFs.

in Table 4. It is revealed that although the values of $C_{1+\alpha}$, and hence f, for these two orders are the same for both Cases 1 and 2, however, (i) the model coefficients are highly dissimilar, and (ii) the two design variables for $\alpha = 0.46$ and one for $\alpha = 0.68$ based on Case 2 are stuck at the lower bound, which does not occur for Case 1. A larger value of MSE is also yielded for Case 2 in comparison to Case 1. This implies that to ensure the constraint $\left|T^{1+\alpha}(j1)\right| = 1/\sqrt{2}$ for Case 2, the optimizer in Step 2 fails to reduce the modeling error throughout the entire bandwidth. This is justified in Figures 6(a)–(b), which show the magnitude comparison plots of the FOBFs based on Cases 1 and 2, for $\alpha = 0.46$ and 0.68, respectively.

Figure 7 presents the magnitude plots of the 1.68^{th}-order FOBF, where the lower frequency bound is 10^{-10} rad/s. The magnitude response of the Case 2 based model deviates from the ideal when the frequency decreases below 0.001 rad/s, with $\left|T^{1.68}(j0.001)\right|$ being –0.3644 dB, while $\left|T^{1.68}(j10^{-10})\right|$ equals to –100.7 dB. It is noteworthy that the magnitude response exhibits a band-pass-like behavior in the range $\omega \in [10^{-10}, 10^{3}]$ rad/s since x_3 is practically zero. However, for the considered bandwidth of approximation $\omega \in [10^{-3}, 10^{3}]$ rad/s, the magnitude response of the approximant exhibits the desired low-pass characteristic.

Figure 8 presents the magnitude at 1 rad/s for the $(1 + \alpha)$-order FOBFs based on Case 1 (*top left*), Case 2 (*top right*), Case 3 (*middle left*), and Case 4 (*middle right*). For Cases 2 and 4, the magnitude is nearly equal to the ideal value of –3.01 dB. This finding demonstrates that the optimizer can effectively satisfy the constraint $\left|T^{1+\alpha}(j1)\right| = 1/\sqrt{2}$ for these two cases. The responses of the designs based on Cases 1 and 3 deviate from the theoretical one due to the absence of such an explicit constraint. Comparison between the magnitude values of the FOBFs at 1 rad/s for Cases 1 and 3 is presented in Figure 8 (*bottom*). It is found that the two

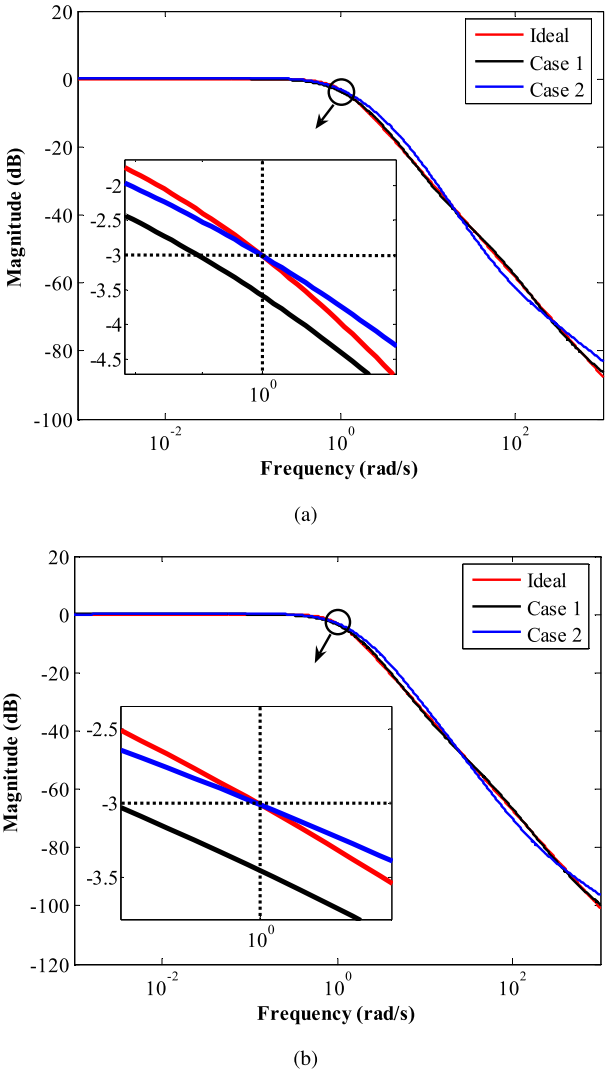

FIGURE 6. Magnitude-frequency comparison plots for the designed FOBFs ($n = 1$) with (a) $\alpha = 0.46$ and (b) $\alpha = 0.68$.

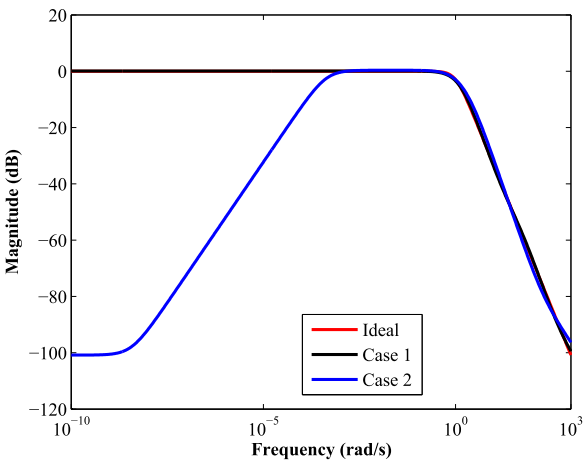

FIGURE 7. Magnitude-frequency comparison plots for the designed FOBF ($n = 1$, $\alpha = 0.68$) for $\omega \in [10^{-10}, 10^{3}]$ rad/s.

responses are similar for all values of α, except for $\alpha = 0.05$ (Case 1: –3.297 dB, Case 3: –3.103 dB), $\alpha = 0.06$

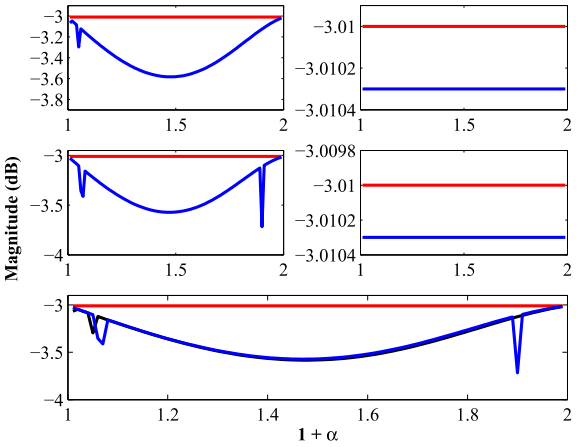

FIGURE 8. Magnitude (dB) at $\omega = 1$ rad/s for the designed FOBFs (*solid blue*) based on Case 1 (*top left*), Case 2 (*top right*), Case 3 (*middle left*), Case 4 (*middle right*), and comparison between Case 1 (*solid black*) and Case 3 (*solid blue*) based FOBFs (*bottom*). The ideal response is shown in *solid red*.

(Case 1: –3.123 dB, Case 3: –3.355 dB), $\alpha = 0.07$ (Case 1: –3.141 dB, Case 3: –3.413 dB), and $\alpha = 0.90$ (Case 1: –3.125 dB, Case 3: –3.718 dB).

Figures 9(a)–(c) show the comparison of MSE for the designed FOBFs based on Case 1 with those of Case 2, Case 3, and Case 4, respectively. It is revealed that: (i) Case 1 achieves the best accuracy among the four cases; (ii) For Case 2, significantly large MSE of 0.3908 dB^2, 2.645 dB^2, and 2.504 dB^2 are yielded for $\alpha = 0.14$, 0.46, and 0.68, respectively; (iii) The value of MSE for Case 3 is marginally higher than Case 1, with a large spike (MSE = 0.4448 dB^2) occurring at $\alpha = 0.90$. The design variable vector X_P for this order is [0.00203465 1.40528707 0.00000778 2.12103022 1.38670144 0.00000778]; zeros are located at –690.6775 and –0.00000553; and poles are located at –1.0605±0.5118i, and –0.00000561. While forcing the model to meet the constraint $\left|T^{n+\alpha}(j0)\right| = 1$, Case 3 for $\alpha = 0.90$ results in the near cancellation of a pole-zero pair located practically at 0; and (iv) For Case 4, the values of MSE at $\alpha = 0.07$ and $\alpha = 0.10$ are 0.1004 dB^2 and 0.2031 dB^2, respectively, which is significantly larger compared to Case 1 (MSE = 0.0069 dB^2 and 0.0139 dB^2). Thus, while additional constraints may allow the designs to meet the ideal magnitude response at 0 and 1 rad/s, however, the trade-off lies in yielding a higher modeling error over the entire bandwidth. From the perspective of design accuracy, Case 1 may be preferred over the other three.

3) COMPARISON WITH THE LITERATURE

Figure 10 presents the MSE comparison plots between the proposed $(1 + \alpha)$-order models with the third-order FOBFs designed using the PSO algorithm with CFE-based substitution [34] and the Powell's algorithm [43]. It can be observed that both the reported designs are significantly outperformed by the proposed method. The maximum value of MSE (MMSE) for [34] is obtained at $\alpha = 0.76$ (MMSE = 36.32 dB^2); for [43], MMSE of 39.46 dB^2 is yielded at $\alpha = 0.94$. In contrast, MMSE of only 0.1981 dB^2 (which occurs at $\alpha = 0.56$) is achieved for the proposed method.

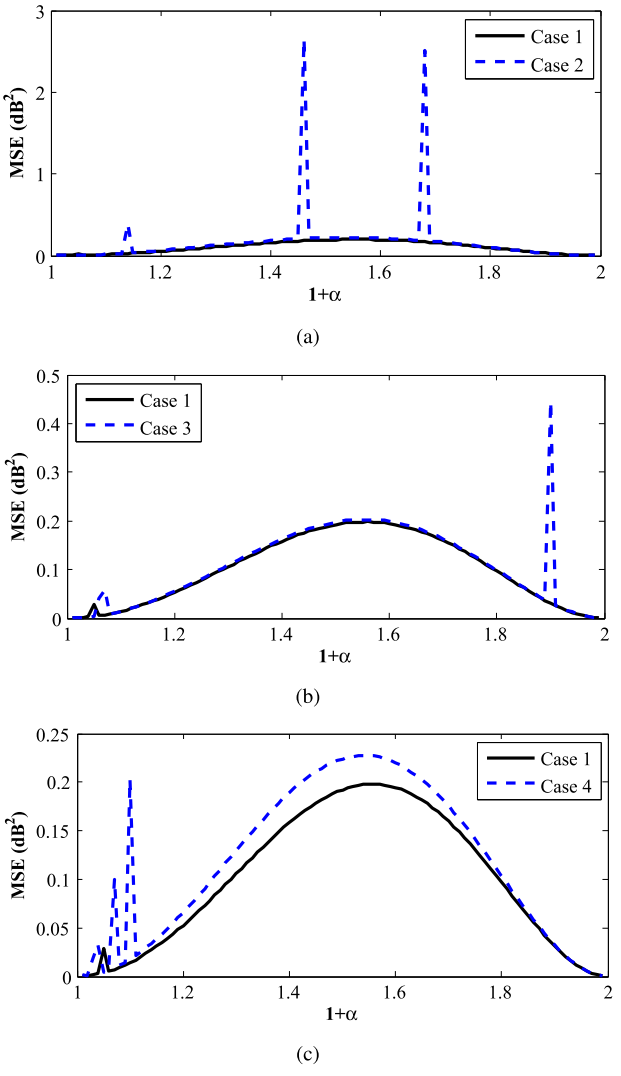

FIGURE 9. Comparison of MSE for the $(1 + \alpha)$-order FOBFs based on Case 1 with the models designed using (a) Case 2, (b) Case 3, and (c) Case 4.

Comparisons of MSE for the proposed models with the optimal $(1+\alpha)$-order FOBFs reported for the same bandwidth in [41], are presented in Figure 11. The same value of MSE is achieved by the proposed designs for all orders, except for $\alpha = 0.05$ where the proposed (0.02907 dB^2) differs from the reported one (0.003542 dB^2). The similarity in MSE between the reported and proposed FOBFs arises due to the closeness of their design variables. Consequently, the proposed FOBFs achieve similar accuracy compared to the state-of-the-art reported in [41]. This fact is highlighted by considering three arbitrarily chosen example cases ($\alpha = 0.2, 0.5, 0.8$), as shown in Table 5.

In contrast, the large variation in X_P for $\alpha = 0.05$ reported in [41] with the proposed one may be noted from Table 5.

TABLE 5. Comparison between the design variables vector.

α	X_P for the Constrained Optimization Method [41]	X_P for the Proposed Method
0.20	[0.2683 55.9756 498.2293 112.4927 632.2146 494.3707]	[0.2703 55.9497 497.8479 112.4298 631.7336 493.9948]
0.50	[0.0357 12.7028 167.3721 70.7972 236.1866 165.3018]	[0.0354 12.6991 167.3206 70.7768 236.1132 165.2506]
0.80	[0.0035 2.8485 58.4866 43.8048 85.2253 58.0271]	[0.0035 2.8485 58.4836 43.8029 85.2207 58.0242]
0.05	[0.7168 119.0177 876.6814 142.5752 1031.1681 874.6902]	[0.7487 29.9201 1E–8 32.9621 29.7615 1E–8]

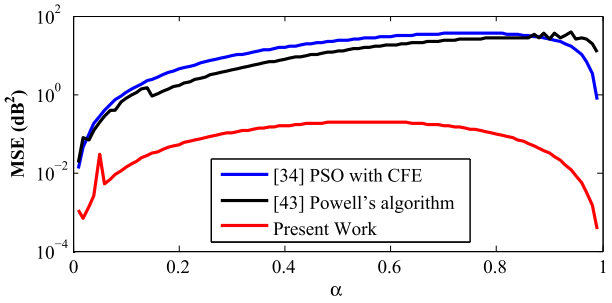

FIGURE 10. MSE comparison plots for the proposed $(1+\alpha)$-order Butterworth filter with the models reported in [34] and [43].

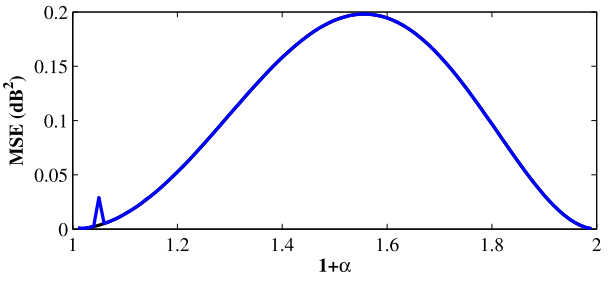

FIGURE 11. MSE comparison plots for the proposed FOBFs (*blue*) with the constrained optimization method cited in [41] (*black*).

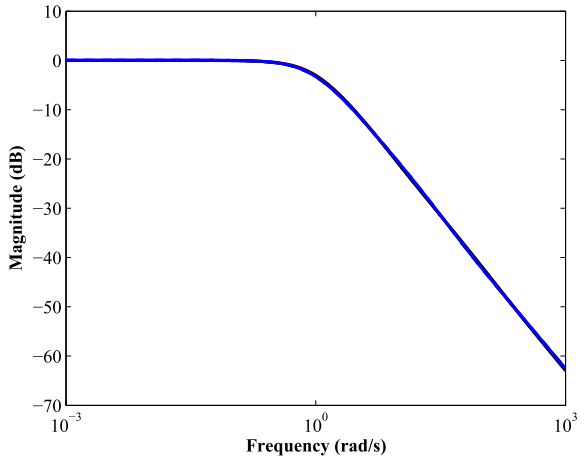

FIGURE 12. Magnitude response comparison plots between the proposed 1.05th-order FOBF $T^{1.05}(s)$ (*solid blue*), $\hat{T}^{1.05}(s)$ (*dashed blue*), the reported model [41] (*solid black*), and the ideal one (*solid red*).

However, it may be observed from Figure 12 that no noticeable difference exists in the magnitude responses between the proposed and reported 1.05th-order models. Moreover, since x_3 and x_6 for the proposed approximant ($\alpha = 0.05$) are

TABLE 6. Optimal design variables vector for $0.01 \leq \alpha \leq 0.06$.

α	X_P
0.01	[0.9437 35.4120 0.0066 36.8982 35.3726 0.0071]
0.02	[0.8780 133.3798 872.6763 143.8144 1019.1039 873.4149]
0.03	[0.8224 129.6030 897.1495 144.7244 1047.8031 896.9678]
0.04	[0.7707 121.9125 837.4030 140.8427 984.9127 838.1239]
0.05	[0.7487 29.9201 1E–8 32.9621 29.7615 1E–8]
0.06	[0.6760 113.1414 841.3961 140.3030 995.2588 839.1339]

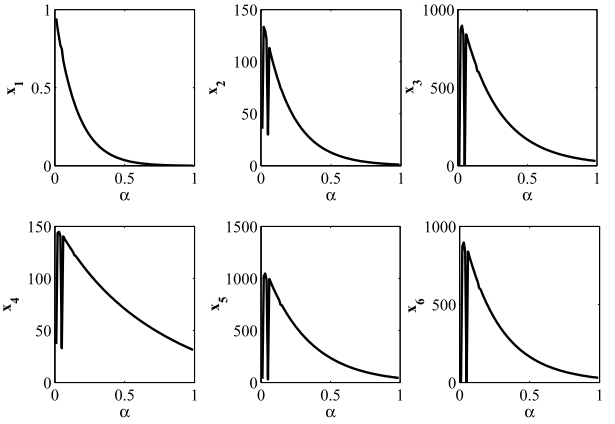

FIGURE 13. Optimal values of coefficients for the proposed $(1+\alpha)$-order FOBFs.

small (1E–8), fixing these values to 0 results in a second-order approximant, as given by (8):

$$\hat{T}^{1.05}(s) = \frac{0.7487s + 29.9201}{s^2 + 32.9621s + 29.7615}. \tag{8}$$

Interestingly, the FOBF as modeled by (8) also attains proximity to the ideal magnitude-frequency behavior of the 1.05th-order Butterworth filter, as illustrated in Figure 12. Both the second-order and third-order proposed approximants for $\alpha = 0.05$ attains the same MSE of 0.029068 dB^2.

4) GENERALIZED EXPRESSIONS OF MODEL COEFFICIENTS

The optimal values of $x_1, x_2, \ldots, x_6$ for the proposed FOBFs (Case 1) are plotted in Figure 13. A significant perturbation exists in x_2 to x_6 for $0.01 \leq \alpha \leq 0.06$, beyond which the values of the coefficients smoothly and monotonically decrease. The optimal values of X_P for $0.01 \leq \alpha \leq 0.06$ are presented in Table 6.

The optimal model coefficients x_i ($i = 1, 2, \ldots, 6$) may be approximated using an m^{th}-degree polynomial in α. As a representative, fitting of the optimal coefficient x_2 using an

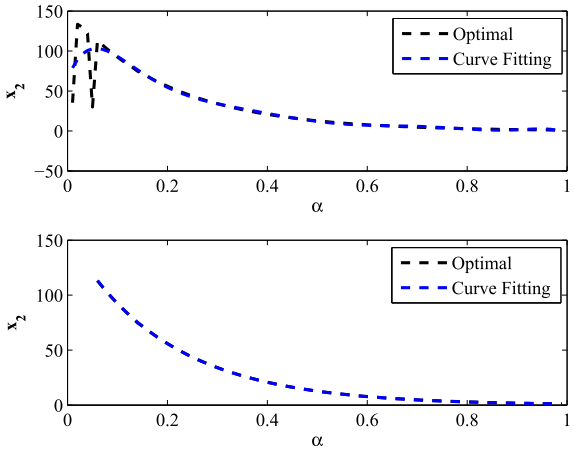

FIGURE 14. Comparison of optimal and 8th-degree polynomial fitted coefficient x_2 for $\alpha \in [0.01, 0.99]$ (*top*) and $\alpha \in [0.06, 0.99]$ (*bottom*).

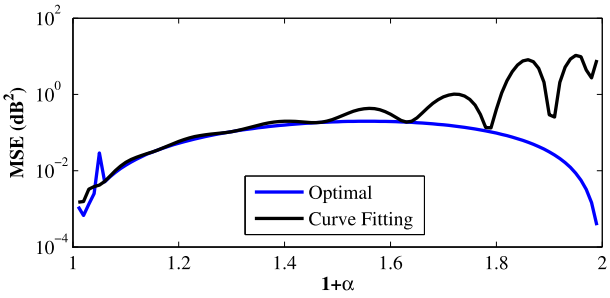

FIGURE 15. Comparison of MSE between the optimal and 8th-degree polynomial fitted coefficients of $(1+\alpha)$-order FOBFs in the range $\alpha \in [0.01, 0.99]$.

8th-degree ($m = 8$) polynomial in α, for $0.01 \leq \alpha \leq 0.99$ (*top*) and $0.06 \leq \alpha \leq 0.99$ (*bottom*) is shown in Figure 14. It can be observed that choosing $\alpha = 0.06$ as the starting value results in improved fitting to the optimal x_2. The norm of residuals (0 in the ideal case) for the curve fitting of x_2 with $\alpha \in [0.01, 0.99]$ and $\alpha \in [0.06, 0.99]$ is 104.49 and 0.634, respectively.

Figure 15 shows that the 8th-degree polynomial fitted coefficients for $0.01 \leq \alpha \leq 0.99$ result in significantly large MSE beyond $\alpha > 0.50$ in comparison to the optimal one. It is noteworthy that even for a 12th-degree polynomial fitting for $\alpha \in [0.01, 0.99]$, the norm of residuals obtained for $x_2, x_3, \ldots, x_6$ are 99.177, 924.63, 116.82, 1053.2, and 923.95, respectively. Thus, due to the observed perturbations, it is difficult to obtain good accuracy based on the generalized expressions for the coefficients starting from $\alpha = 0.01$. Therefore, the curve fitting of the optimal coefficients needs to be carried out in the range $\alpha \in [0.06, 0.99]$.

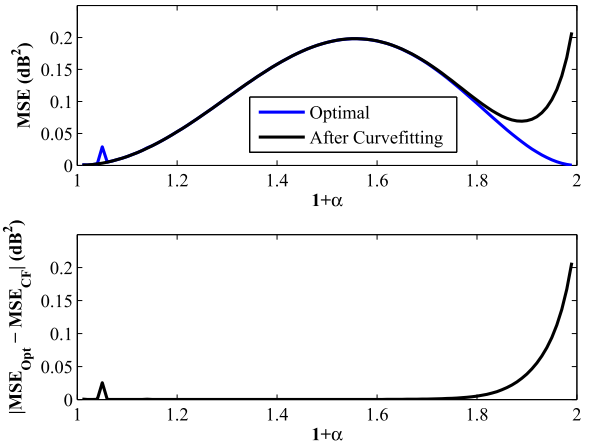

FIGURE 16. Comparison of MSE between the optimal FOBF and the model obtained as per (9) for $\alpha \in [0.01, 0.99]$.

The norm of residuals yielded for different values of m for $\alpha \in [0.06, 0.99]$ are presented in Table 7. It is found that increasing m results in a smaller norm of residuals for all coefficients. The generalized expressions for the 8th-degree polynomial fitted coefficients of $T^{1+\alpha}(s)$, where $\alpha \in [0.06, 0.99]$, are presented as a matrix equation in (9), as shown at the bottom of the page.

Figure 16 (*top*) shows the MSE plots for the FOBF modeled using (9) compared to the optimal one, for $\alpha \in [0.01, 0.99]$. The corresponding absolute difference in MSE obtained using the optimal (MSE_{Opt}) and curve fitted (MSE_{CF}) models is presented in Figure 16 (*bottom*). It is revealed that: (i) the model based on (9) achieves a lower MSE (0.003554 dB^2) compared to the optimal (0.02907 dB^2) 1.05th-order FOBF. After polynomial fitting, the decision variables for the 1.05th-order approximant is yielded as $X_P = [0.7215\ 119.1411\ 876.6214\ 142.7952\ 1031.5836\ 874.2710]$ which avoids the value of 1E–8 obtained for x_3 and x_6 in the optimal case, and (ii) the MSE achieved by the curve fitted and optimal models are similar up to $\alpha \leq 0.80$.

$$\begin{bmatrix} x_1 \\ x_2 \\ x_3 \\ x_4 \\ x_5 \\ x_6 \end{bmatrix} = \begin{bmatrix} 3.4390 & -18.8117 & 45.8370 & -66.2936 & 63.9512 & -43.4402 & 20.8045 & -6.4848 & 0.9988 \\ 492.96 & -2529.8 & 5695.9 & -7535.8 & 6710.9 & -4408.9 & 2225.4 & -803.82 & 154.28 \\ 7607.6 & -36774 & 75316 & -85751 & 60820 & -29925 & 12151 & -4489.4 & 1074.1 \\ 486.81 & -2426.2 & 5059.2 & -5739.5 & 3881.2 & -1666.9 & 568.62 & -288.41 & 155.98 \\ 9481.6 & -45639 & 92724 & -103780 & 70826 & -32184 & 11914 & -4527.8 & 1231.8 \\ 6481.4 & -31434 & 64716 & -74387 & 53779 & -27463 & 11734 & -4468.9 & 1071.5 \end{bmatrix} \cdot \begin{bmatrix} \alpha^8 \\ \alpha^7 \\ \alpha^6 \\ \alpha^5 \\ \alpha^4 \\ \alpha^3 \\ \alpha^2 \\ \alpha \\ 1 \end{bmatrix} \quad (9)$$

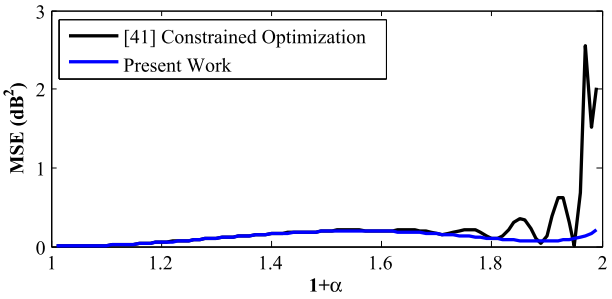

FIGURE 17. Comparison of MSE between the proposed and reported curve fitted $(1+\alpha)$-order FOBFs.

TABLE 7. Norm of residuals for coefficients ($\alpha \in [0.06,\ 0.99]$).

m	Norm of residuals for					
	x_1	x_2	x_3	x_4	x_5	x_6
2	0.40294	49.411	242.90	8.3865	216.85	246.57
3	0.1379	14.264	58.767	1.8877	47.377	59.632
4	0.039202	3.6012	20.832	1.332	22.693	19.108
5	0.0095419	1.0533	16.944	1.2935	20.654	14.604
6	0.0021062	0.67209	16.459	1.278	20.234	14.111
7	0.00048455	0.63657	16.303	1.2654	20.049	13.972
8	0.00030239	0.63426	16.281	1.2643	20.022	13.954
9	0.00028546	0.63376	16.265	1.2635	20.003	13.940
10	0.00028268	0.62867	16.133	1.2521	19.841	13.826
11	0.00027745	0.62001	15.912	1.2363	19.569	13.636
12	0.00027503	0.61315	15.734	1.2215	19.351	13.484

In [41], generalized expressions of coefficients based on the 12th-degree polynomial fitting for the $(1+\alpha)$ order FOBFs were reported. Figure 17 presents the MSE ($\alpha \in [0.01,\ 0.99]$) comparison plots for the proposed curve fitted approximants with their corresponding counterparts cited in [41]. It may be observed that the proposed approach can achieve superior modeling accuracy (lower MSE) over [41] beyond $\alpha \geq 0.61$. The MMSE attained at $\alpha = 0.97$ for the reported method [41] is 2.551 dB^2, while the proposed FOBF yields only 0.140 dB^2.

B. DESIGN OF FOBFs FOR n > 1

The applicability of the proposed technique towards the optimal modeling of higher-order FOBFs is demonstrated in this section. Figure 18 shows the optimal values of the design variables obtained for FOBFs with $n = 2$. However, polynomial curve fitting with a lower norm of residuals may not be achieved due to the large variations throughout the design range for the optimal coefficients (x_2 to x_9).

Figure 19 presents the optimal values of $C_{2+\alpha}$ (*top*), f (*middle*), and MSE (*bottom*) achieved for the $(2+\alpha)$-order FOBFs. It is found that (i) the profile yielded for $C_{2+\alpha}$ is similar to that obtained for $C_{1+\alpha}$; (ii) the worst value of f (14.33 dB^2) occurs at $\alpha = 0.58$, although the MSE (0.01178 dB^2) is significantly small; (iii) At $\alpha = 0.89$, $C_{2+\alpha}$ is obtained as 0, which implies that the resultant initial point is the transfer function of the third-order Butterworth filter. Hence, a large peak for f (7.273 dB^2) is exhibited with the 2.89th-order filter; however, the resultant MSE is low (0.002083 dB^2); and

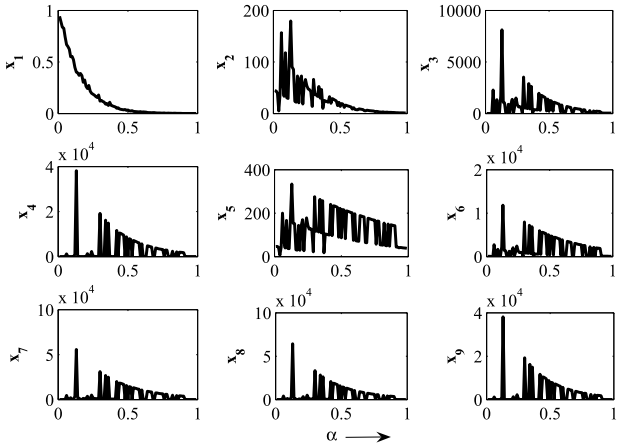

FIGURE 18. Optimal values of coefficients for the proposed $(2+\alpha)$-order FOBFs.

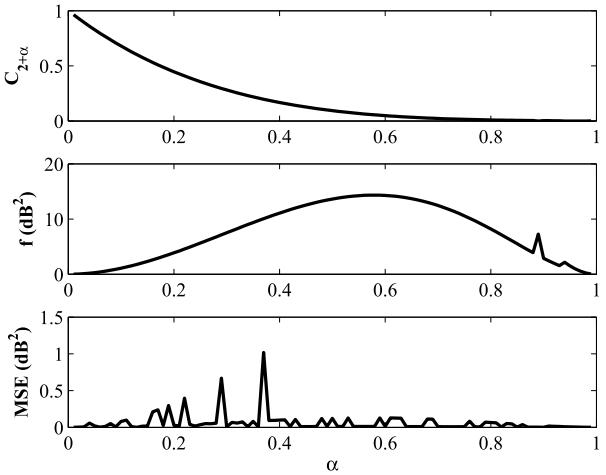

FIGURE 19. $C_{n+\alpha}$ (*top*), f (*middle*), and MSE (*bottom*) plots for the proposed FOBFs with $n = 2$.

(iv) three particular orders, namely $\alpha = \{0.22, 0.29, 0.37\}$, yield an abrupt peaking in MSE as coefficient x_3 attains a value of 1E–8. However, the corresponding values of f and MSE are {4.563, 7.134, 10.070} dB^2 and {0.3966, 0.6698, 1.0180} dB^2, respectively, which demonstrates a reduction by a factor of approximately 10 in the modeling error.

Table 8 presents the values of $C_{n+\alpha}$, f, X_P, and MSE for the proposed $(2+\alpha)$ and $(3+\alpha)$-order FOBFs, with $\alpha = 0.2$, 0.5, and 0.8. A considerable reduction in error (by more than a factor of 100) is obtained for the considered approximants going from Step 1 to Step 2 of the proposed optimization procedure. The magnitude-frequency plots of the initial point and optimal models for these test cases are illustrated in Figures 20(a)–(b) for $n = 2$ and $n = 3$, respectively. The response of the initial point deviates from the ideal behavior; however, the optimal approximant achieves good agreement for all cases. Thus, the proposed technique also demonstrates an efficient modeling performance for the design of higher-order FOBFs.

TABLE 8. Optimal design variables and error values for the proposed FOBFs ($n = 2, 3$).

$n+\alpha$	$C_{n+\alpha}$	f (dB^2)	X_P	MSE (dB^2)
2.2	0.4466	3.8752	[0.2643 66.5312 876.7349 56.9033 142.3547 1224.5916 1417.8851 974.6678 56.7873]	0.0288
2.5	0.0938	13.6214	[0.0341 13.7755 238.9280 0.7127 86.5720 412.7966 395.2263 242.7884 0.7074]	0.1231
2.8	0.0093	8.2005	[0.0034 2.9312 75.2191 0.2528 53.4711 147.3821 138.7575 76.2588 0.2517]	0.0661
3.2	0.4465	3.8596	[0.2614 72.4680 1146.1898 77.2059 1213.8499 160.1420 1715.5370 2817.7762 4383.1554 3950.9360 2714.2397 1210.6682]	0.0210
3.5	0.0938	13.5990	[0.0332 14.6562 312.5331 19.6886 46.3822 100.8941 637.5639 858.2614 907.9462 470.7962 131.3232 46.1691]	0.0869
3.8	0.0093	8.1973	[0.0033 2.9916 89.6395 1.2450 45.6250 61.5808 221.5039 306.4617 345.5887 229.7347 118.4787 45.4683]	0.0495

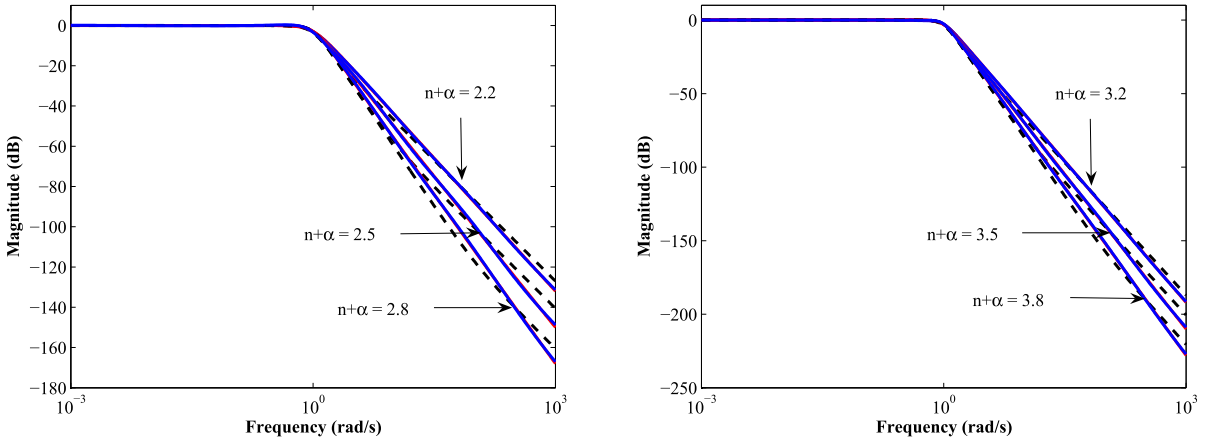

FIGURE 20. Magnitude response comparison plots between the ideal (*solid red*), initial point (*dashed black*), and proposed FOBFs (*solid blue*) for (a) $n = 2$, and (b) $n = 3$.

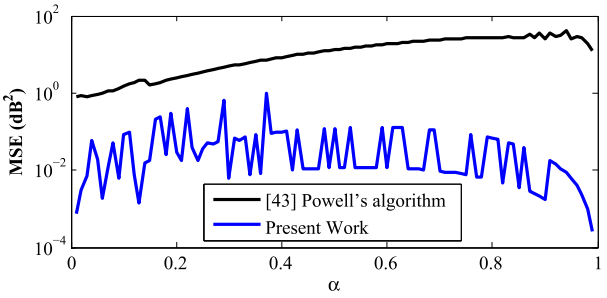

FIGURE 21. MSE comparison plots for the proposed $(2+\alpha)$-order FOBFs with the literature.

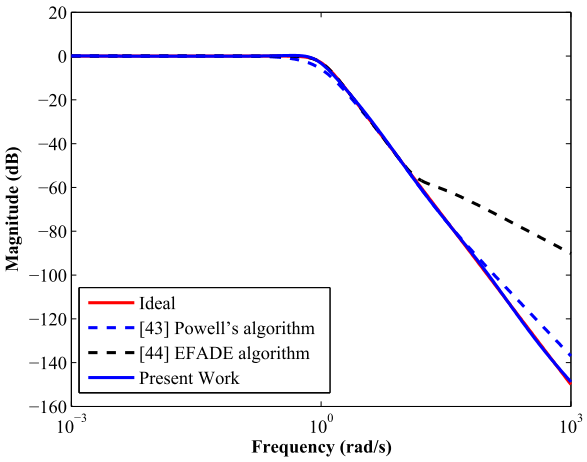

FIGURE 22. Magnitude-frequency comparison plots of the proposed 2.5$^{\text{th}}$-order FOBF with the literature.

For the Enhanced Fitness Adaptive Differential Evolution (EFADE) algorithm based FOBFs of order {2.1, 2.2, …, 2.9} reported in [44], the MSE values are obtained as {55.751, 163.348, 284.368, 372.299, 394.465, 469.482, 530.430, 654.157, 938.962} dB^2. In contrast, the proposed method achieves a significantly lower MSE of {0.081, 0.029, 0.006, 0.098, 0.123, 0.011, 0.009, 0.006, 0.001} dB^2. Figure 21 shows the MSE comparison plots between the proposed and Powell's algorithm [43] based $(2+\alpha)$-order FOBFs for α varying from 0.01 to 0.99 in steps of 0.01. It is observed that the proposed method can significantly outperform [43] throughout the design range. The magnitude response of the proposed 2.5$^{\text{th}}$-order FOBF is compared with the recent literature, as shown in Figure 22. The responses of the models reported in [43] and [44] appreciably deviate from the theoretical characteristic beyond 75.31 rad/s and 12.83 rad/s, respectively. In contrast, the proposed approximant remains in proximity to the ideal magnitude response throughout the bandwidth.

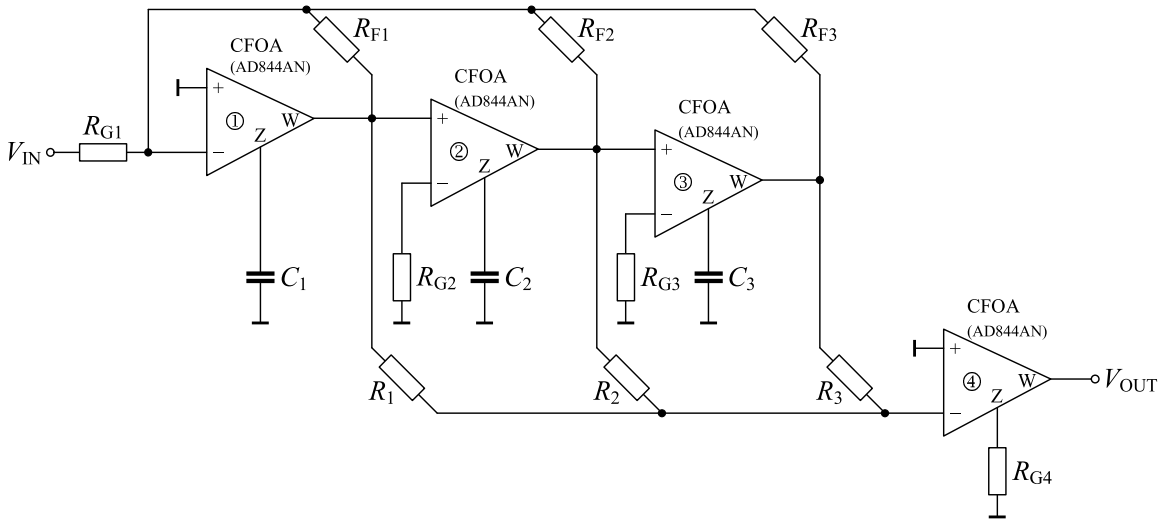

FIGURE 23. CFOA-based circuit realization of the proposed $(1+\alpha)$-order Butterworth filter.

C. CIRCUIT REALIZATION

CFOAs have been employed as active elements to realize the FO filters in several research works [48], [49]. Figure 23 shows the circuit diagram to realize the proposed $(1+\alpha)$-order Butterworth filter using the CFOAs in follow-the-leader feedback topology. The complexity of the proposed filter circuit is reasonable since the $(1+\alpha)$-order FOBF is implemented using a third-order circuit. The circuit transfer function in voltage mode is defined according to (10):

$$\frac{V_{OUT}(s)}{V_{IN}(s)} = \frac{\frac{R_{G4}}{R_1R_{G1}C_1}s^2 + \frac{R_{G4}}{R_2R_{G1}R_{G2}C_1C_2}s + \frac{R_{G4}}{R_3R_{G1}R_{G2}R_{G3}C_1C_2C_3}}{s^3 + \frac{1}{R_{F1}C_1}s^2 + \frac{1}{R_{G2}R_{F2}C_1C_2}s + \frac{1}{R_{G2}R_{G3}R_{F3}C_1C_2C_3}}. \quad (10)$$

The circuit realization of the proposed (normalized) 1.5^{th}-order FOBF modeled using (9), as given by (11):

$$T^{1.5}(s) = \frac{0.0354s^2 + 12.7050s + 167.2891}{s^3 + 70.7800s^2 + 236.1953s + 165.1961}, \quad (11)$$

is considered for demonstration purposes. The design cut-off frequency is chosen as 1 kHz. Comparing (10) with the frequency transformation to 1 kHz of (11), leads to 6 design equations involving 13 unknown parameters. The resistor and capacitor values are selected from the E–24 and E–12 standard industrial series, respectively. The following components are initially set: $R_{G1} = 20$ kΩ, $R_{G2} = 1$ kΩ, $R_{G3} = 1$ kΩ, $R_{G4} = 1$ kΩ, $R_{F1} = 1$ kΩ, $R_{F2} = 5.1$ kΩ, and $R_{F3} = 100$ kΩ. The standard values for the remaining components are derived as: $R_1 = 100$ kΩ, $R_2 = 4.7$ kΩ, $R_3 = 4.7$ kΩ, $C_1 = 2.2$ nF, $C_2 = 10$ nF, and $C_3 = 12$ nF.

1) SPICE SIMULATION

Simulations are conducted in OrCAD PSPICE software with the AD844A/AD IC employed as CFOA. Figure 24 shows the magnitude response of the MATLAB and SPICE simulated

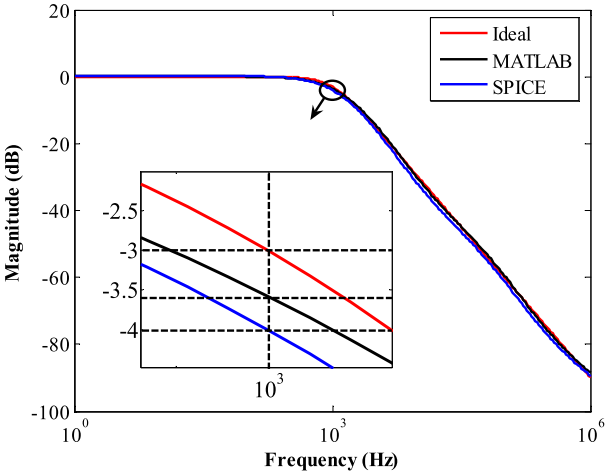

FIGURE 24. Magnitude-frequency responses of the proposed 1.5^{th}-order FOBF.

FOBF circuit, which demonstrates good agreement with the ideal (given by (1), with $\omega_C = 2000\pi$ rad/s) characteristics throughout the design bandwidth. The magnitude of the SPICE simulated proposed circuit implementation at 1 kHz (Mag@1kHz) is –4.009 dB, while MATLAB simulation yields –3.585 dB, as shown by the zoomed-in plot in Figure 24. The Monte-Carlo simulations, considering 5% and 10% tolerance values (drawn from a Gaussian distribution) for the resistors and capacitors, respectively, with fixed random number seed value 17533 were performed for 200 runs. The corresponding magnitude responses, as presented in Figure 25, further validate the closeness to the theoretical expectations. Various statistical indices concerning the Mag@1kHz and the frequency (Hz) value at –3 dB magnitude of the FOBF (Freq@–3dB) are also determined using the Monte-Carlo simulations. The {minimum, maximum, mean, standard deviation (SD)} indices for Mag@1kHz and

TABLE 9. Monte-Carlo simulation based statistical results for the frequency (Hz) at –3 dB magnitude due to variation of RC components.

Index	Frequency (Hz) at –3 dB magnitude due to variation of												
	C_1	C_2	C_3	R_1	R_2	R_3	R_{F1}	R_{F2}	R_{F3}	R_{G1}	R_{G2}	R_{G3}	R_{G4}
Min	799.74	763.15	619.71	800.56	799.91	799.65	783.29	681.40	699.28	800.58	783.49	705.15	800.59
Max	801.50	837.52	1083.32	800.61	801.465	801.61	819.61	939.97	922.40	800.59	818.30	913.29	800.59
Mean	800.62	801.90	801.67	800.59	800.58	800.63	800.10	807.06	798.49	800.59	801.27	798.45	800.59
SD	0.3739	15.9556	96.8547	0.0114	0.3290	0.4172	7.7346	55.0252	47.3132	5E–04	7.4134	44.1603	4E–05

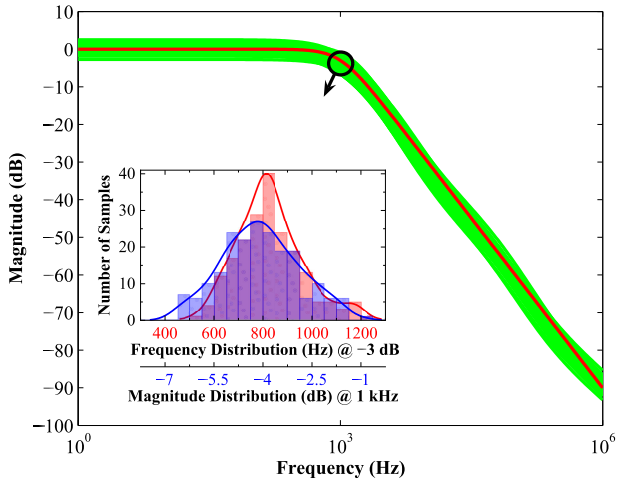

FIGURE 25. Magnitude-frequency responses of the ideal (*red*) and Monte-Carlo simulated (*green*) 1.5th-order FOBF.

Freq@–3dB are obtained as {–6.618, –0.967, –4.070, 1.176} dB, and {520.621, 1215.417, 827.538, 134.456} Hz, respectively. The Monte-Carlo histograms for the Mag@1kHz and Freq@–3dB are presented as an inset in Figure 25.

Monte-Carlo simulations with fixed random number seed value 17533 were also conducted to determine the effects on the Freq@–3dB and Mag@1kHz due to the variation of each of the RC components for the proposed circuit. To demonstrate the results, Figures 26(a)-(b) present the box plots concerning the Freq@–3dB and Mag@1kHz metrics, respectively. In the case of Freq@–3dB, it is found that: (i) capacitor C_3 results in the largest SD (96.8547 Hz), followed by the resistors R_{F2} (55.0252 Hz), R_{F3} (47.3132 Hz), and R_{G3} (44.1603 Hz); (ii) the least values of SD are attained by R_{G4} (4.048×10^{-5} Hz) and R_{G1} (5.646×10^{-4} Hz); and (iii) the mean value is around 800 Hz for all the cases, except for R_{F2}, which yields 807.06 Hz. Table 9 presents the detailed statistical results concerning the influence of the passive components on the Freq@–3dB metric. In the case of Mag@1kHz, it is revealed that: (i) among all the components, C_3 yields the largest SD (0.6885 dB); (ii) among the resistors, R_{G1} (0.4227 dB) attains the largest SD, followed by R_{G4} (0.4226 dB), R_3 (0.4133 dB), R_{F2} (0.3897 dB), and R_{G3} (0.3258 dB); (iii) the smallest value of SD is achieved by R_1 (0.0004 dB); and (iv) for all the cases, the mean value of Mag@1kHz is around –4 dB. The statistical performance indices in this regard are presented in Table 10.

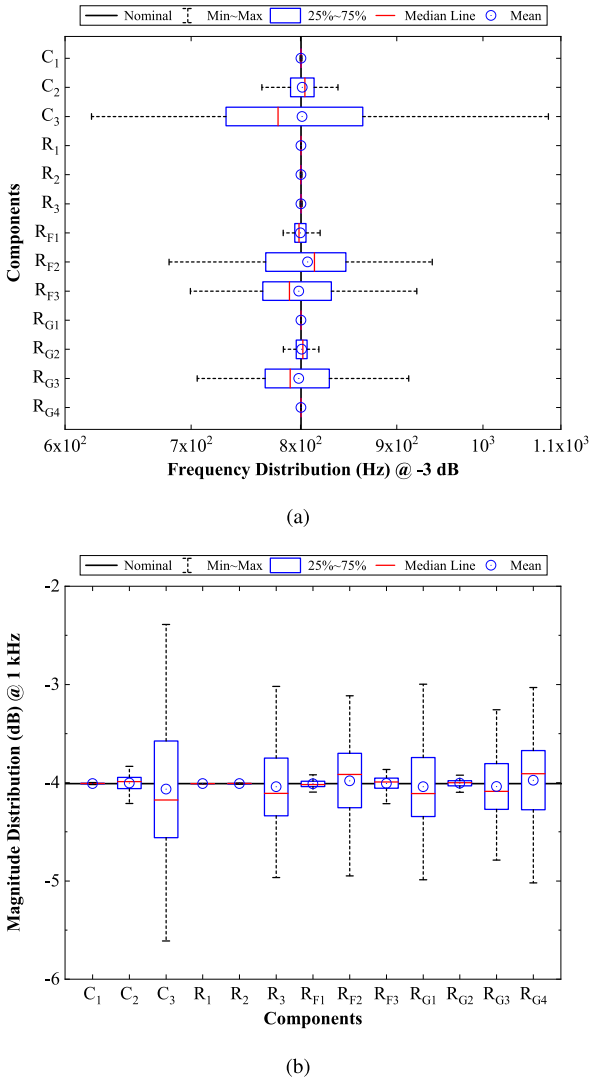

FIGURE 26. Passive component effects on Monte-Carlo simulated (a) frequency distribution at –3 dB, (b) magnitude distribution at 1 kHz of the proposed 1.5th-order FOBF.

Figure 27 presents the SPICE simulated worst-case sensitivity plots concerning the magnitude (*top*) and the absolute relative magnitude error (ARME) (*bottom*) for the 1.5th-order model. It may be observed that: (i) the magnitude response of the proposed FOBF based on the nominal values of components lies in-between those of the worst-case (Hi, Low) plots; and (ii) the maximum value of ARME (MARME) for the worst-case sensitivity performance of the proposed FOBF is 0.4738, which occurs at 9550 Hz. In contrast, an MARME

TABLE 10. Monte-Carlo simulation based statistical results for the magnitude (dB) at 1 kHz due to variation of RC components.

Index	Magnitude (dB) at 1 kHz due to variation of												
	C_1	C_2	C_3	R_1	R_2	R_3	R_{F1}	R_{F2}	R_{F3}	R_{G1}	R_{G2}	R_{G3}	R_{G4}
Min	–4.018	–4.210	–5.611	–4.010	–4.015	–4.965	–4.096	–4.949	–4.213	–4.987	–4.097	–4.788	–5.020
Max	–3.999	–3.833	–2.389	–4.008	–4.003	–3.020	–3.919	–3.115	–3.865	–2.997	–3.922	–3.257	–3.031
Mean	–4.008	–4.004	–4.065	–4.009	–4.009	–4.040	–4.012	–3.980	–4.008	–4.041	–4.006	–4.039	–3.976
SD	0.0040	0.0809	0.6885	0.0004	0.0025	0.4133	0.0378	0.3897	0.0736	0.4227	0.0372	0.3258	0.4226

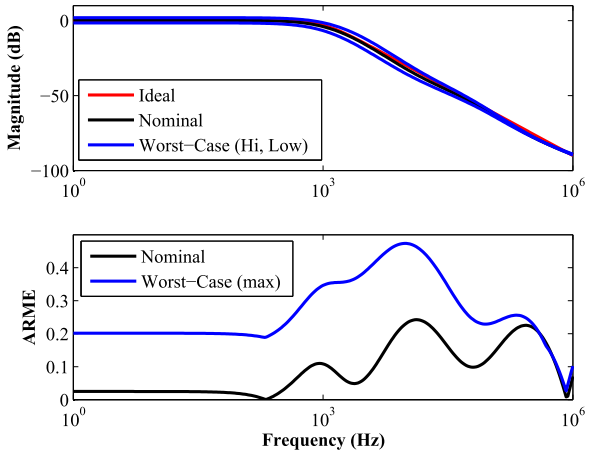

FIGURE 27. Magnitude and absolute relative magnitude error plots of the proposed 1.5th-order FOBF for the worst-case sensitivity.

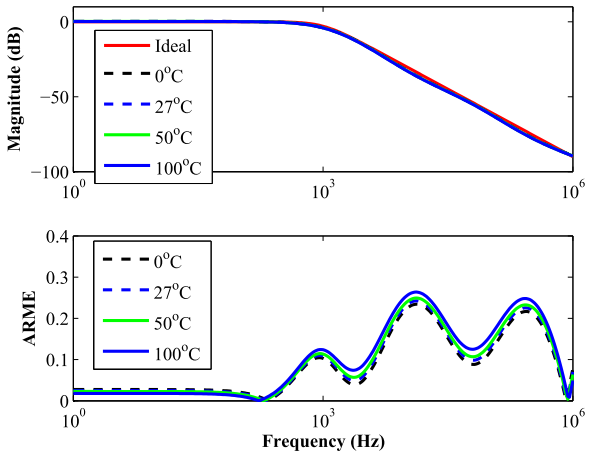

FIGURE 28. Magnitude and absolute relative magnitude error plots of the proposed 1.5th-order FOBF for the temperature sensitivity.

of 0.2424 at 13180 Hz is attained for the design based on the nominal values of components. The R^2 metric relative to the ideal magnitude values obtained for 301 logarithmically spaced points for the FOBFs based on the nominal and worst-case conditions are 0.996792 and 0.927132, respectively.

The temperature sensitivity of the proposed circuit (using the nominal values of RC components) is investigated for various values, such as 0°C, 27°C, 50°C, and 100°C. In Figure 28, the SPICE simulated temperature sensitivity plots of the magnitude (*top*) and ARME (*bottom*) for the

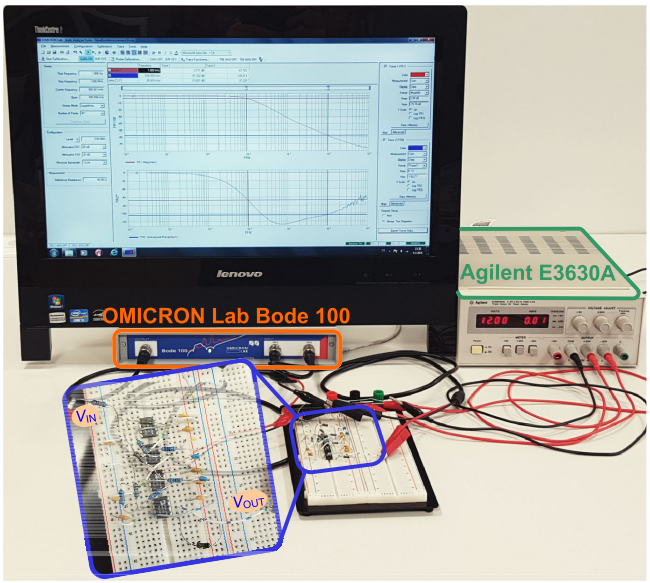

FIGURE 29. Photo of the experimental set-up.

1.5th-order designed FOBF are presented. It is found that the magnitude and ARME responses of the circuit for the four temperature conditions exhibit proximity. Comparisons about R^2 for the magnitude response of the proposed FOBF (evaluated at 301 points with logarithmic spacing) at temperatures of {0°C, 27°C, 50°C, 100°C} relative to the ideal one are obtained as {0.996934, 0.996792, 0.996667, 0.996385}, respectively.

2) EXPERIMENTAL MEASUREMENT

The photograph of the hardware set-up is presented in Figure 29. In experiments, through hole KOA Speer Electronics MF, MFS, RK general purpose metal film resistors with 5% and KEMET Goldmax 300 series multilayer ceramic capacitors with 10% tolerance were used. The supply voltage for Analog Devices AD844AN amplifiers was provided by the Agilent E3630A power supply. The frequency responses of the FOBF were measured by the OMICRON Lab Bode 100 network analyzer and displayed using the Bode Analyzer Suite software. 301 logarithmically spaced frequency points in the range 1 Hz to 1 MHz were considered. The level of the testing harmonic signal was set to 0 dBm (632.46 mV_{pp} or 223.61 mV_{rms}). The receiver bandwidth of the analyzer was fixed at 1 kHz to obtain precise results. Prior to measurements, the THRU calibration of the analyzer was

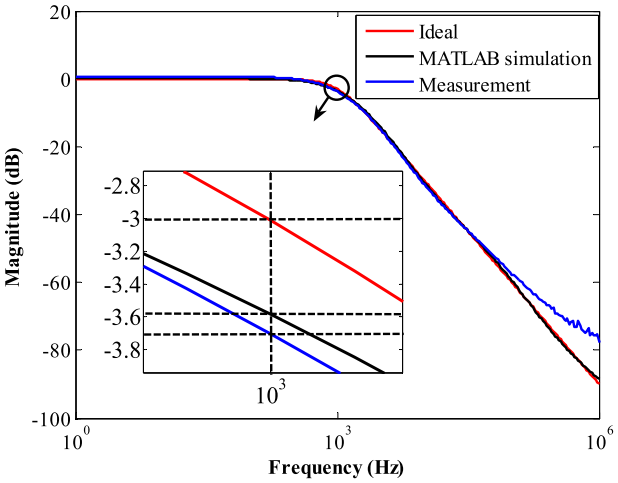

FIGURE 30. Magnitude plot of the proposed CFOA-based 1.5^{th}-order FOBF.

performed to eliminate the influence of the measurement setup. The magnitude response of the practical filter, as shown in Figure 30, demonstrates an excellent agreement with the ideal one up to nearly 75 kHz. The Mag@1kHz for the hardware measurement (–3.704 dB) conforms with the ideal (–3.010 dB), MATLAB (–3.585 dB), and SPICE (–4.009 dB) simulations. R^2 of 0.9947 is achieved for the measured magnitude response data compared to the theoretical one. Thus, the hardware experimental results also validate the practical efficacy of the proposed approach.

IV. CONCLUSION

The concept of an optimal interpolation of the magnitude responses for the classical n^{th} and $(n+1)^{\text{th}}$-order Butterworth filters is introduced to achieve the characteristics of the $(n+\alpha)^{\text{th}}$-order Butterworth filter. In the first step of the proposed design strategy, the optimal value of weighting factors concerning the sum of the n^{th}-order and the $(n+1)^{\text{th}}$-order Butterworth filters are determined. The model from the first step is then treated as an initial point for a constrained optimization routine in the second step in order to determine the coefficients of the proposed rational approximant. In both the design steps, the minimization of the objective function is carried out concerning the magnitude-frequency characteristics of the ideal $(n+\alpha)^{\text{th}}$-order Butterworth filter. The proposed technique does not require (i) the fractional-order transfer function model of the FOBF, (ii) an integer-order approximation of the s^{α} operator, and (iii) cascading of the $(1+\alpha)^{\text{th}}$-order Butterworth filter with the n^{th}-order Butterworth filter to attain the characteristics of the higher-order FOBFs. Effects due to the incorporation of various design constraints on the modeling performance of the proposed approximants are extensively investigated. The best accuracy for the proposed FOBF is achieved for the case $D_{1+\alpha} = 1 - C_{1+\alpha}$ in Step 1, with incorporation of stability constraints in Step 2. The generality of the suggested technique towards the design of higher-order FOBFs is demonstrated. The superior accuracy of the proposed FOBFs over the state-of-the-art designs for six decades of bandwidth is highlighted by a lower value of MSE metric. Discrete components based implementation of the proposed FOBFs using the CFOAs employed as an active element is presented. SPICE simulations and experimental measurements for the 1.5^{th}-order design confirm a good agreement with the ideal magnitude-frequency characteristic. Future work will deal with the on-chip CMOS implementation of the proposed models.

REFERENCES

[1] H. Sun, Y. Zhang, D. Baleanu, W. Chen, and Y. Chen, "A new collection of real world applications of fractional calculus in science and engineering," *Commun. Nonlinear Sci. Numer. Simul.*, vol. 64, pp. 213–231, Nov. 2018, doi: 10.1016/j.cnsns.2018.04.019.

[2] A. Elwakil, "Fractional-order circuits and systems: An emerging interdisciplinary research area," *IEEE Circuits Syst. Mag.*, vol. 10, no. 4, pp. 40–50, Nov. 2010, doi: 10.1109/MCAS.2010.938637.

[3] K. Biswas, G. Bohannan, R. Caponetto, A. M. Lopes, and J. A. T. Machado, *Fractional-Order Devices*. New York, NY, USA: Springer, 2017.

[4] G. Tsirimokou, C. Psychalinos, and A. S. Elwakil, *Design of CMOS Analog Integrated Fractional-Order Circuits: Applications in Medicine and Biology*. Berlin, Germany: Springer, 2017.

[5] T. Helie, "Simulation of fractional-order low-pass filters," *IEEE/ACM Trans. Audio, Speech, Lang. Process.*, vol. 22, no. 11, pp. 1636–1647, Nov. 2014, doi: 10.1109/TASLP.2014.2323715.

[6] A. G. Radwan, A. M. Soliman, and A. S. Elwakil, "First-order filters generalized to the fractional domain," *J. Circuits, Syst. Comput.*, vol. 17, no. 1, pp. 55–66, Feb. 2008, doi: 10.1142/S0218126608004162.

[7] A. G. Radwan, A. S. Elwakil, and A. M. Soliman, "On the generalization of second-order filters to the fractional-order domain," *J. Circuits, Syst. Comput.*, vol. 18, no. 2, pp. 361–386, Apr. 2009, doi: 10.1142/S0218126609005125.

[8] A. S. Ali, A. G. Radwan, and A. M. Soliman, "Fractional order Butterworth filter: Active and passive realizations," *IEEE J. Emerg. Sel. Topics Circuits Syst.*, vol. 3, no. 3, pp. 346–354, Sep. 2013, doi: 10.1109/JETCAS.2013.2266753.

[9] T. Freeborn, B. Maundy, and A. S. Elwakil, "Approximated fractional order Chebyshev lowpass filters," *Math. Problems Eng.*, vol. 2015, Mar. 2015, Art. no. 832468, doi: 10.1155/2015/832468.

[10] A. M. Abdelaty, A. Soltan, W. A. Ahmed, and A. G. Radwan, "On the analysis and design of fractional-order Chebyshev complex filter," *Circuits, Syst., Signal Process.*, vol. 37, no. 3, pp. 915–938, Mar. 2018, doi: 10.1007/s00034-017-0570-1.

[11] T. J. Freeborn, A. S. Elwakil, and B. Maundy, "Approximated fractional-order inverse Chebyshev lowpass filters," *Circuits, Syst., Signal Process.*, vol. 35, no. 6, pp. 1973–1982, Jun. 2016, doi: 10.1007/s00034-015-0222-2.

[12] D. Kubanek, T. J. Freeborn, J. Koton, and J. Dvorak, "Validation of fractional-order lowpass elliptic responses of $(1+s^{\alpha})$-order analog filters," *Appl. Sci.*, vol. 8, no. 12, p. 2603, 2018, doi: 10.3390/app8122603.

[13] S. Kapoulea, C. Psychalinos, and A. S. Elwakil, "Power law filters: A new class of fractional-order filters without a fractional-order Laplacian operator," *AEU Int. J. Electron. Commun.*, vol. 129, Feb. 2021, Art. no. 153537, doi: 10.1016/j.aeue.2020.153537.

[14] S. Kapoulea, C. Psychalinos, and A. S. Elwakil, "Double exponent fractional-order filters: Approximation methods and realization," *Circuits, Syst., Signal Process.*, vol. 40, no. 2, pp. 993–1004, Feb. 2021, doi: 10.1007/s00034-020-01514-7.

[15] L. A. Said, S. M. Ismail, A. G. Radwan, A. H. Madian, M. F. A. El-Yazeed, and A. M. Soliman, "On the optimization of fractional order low-pass filters," *Circuits, Syst., Signal Process.*, vol. 35, no. 6, pp. 2017–2039, Jun. 2016, doi: 10.1007/s00034-016-0258-y.

[16] P. Ahmadi, B. Maundy, A. S. Elwakil, and L. Belostotski, "High-quality factor asymmetric-slope band-pass filters: A fractional-order capacitor approach," *IET Circuits, Devices Syst.*, vol. 6, no. 3, pp. 187–197, May 2012, doi: 10.1049/iet-cds.2011.0239.

[17] D. Kubanek, T. Freeborn, and J. Koton, "Fractional-order band-pass filter design using fractional-characteristic specimen functions," *Microelectron. J.*, vol. 86, pp. 77–86, Apr. 2019, doi: 10.1016/j.mejo.2019.02.020.

[18] J. Baranowski, M. Pauluk, and A. Tutaj, "Analog realization of fractional filters: Laguerre approximation approach," *AEU Int. J. Electron. Commun.*, vol. 81, pp. 1–11, Nov. 2017, doi: 10.1016/j.aeue.2017.06.011.

[19] Z. M. Shah, M. Y. Kathjoo, F. A. Khanday, K. Biswas, and C. Psychalinos, "A survey of single and multi-component fractional-order elements (FOEs) and their applications," *Microelectron. J.*, vol. 84, pp. 9–25, Feb. 2019, doi: 10.1016/j.mejo.2018.12.010.

[20] K. Biswas, R. Caponetto, G. Di Pasquale, S. Graziani, A. Pollicino, and E. Murgano, "Realization and characterization of carbon black based fractional order element," *Microelectron. J.*, vol. 82, pp. 22–28, Dec. 2018, doi: 10.1016/j.mejo.2018.10.008.

[21] G. Tsirimokou, A. Kartci, J. Koton, N. Herencsar, and C. Psychalinos, "Comparative study of discrete component realizations of fractional-order capacitor and inductor active emulators," *J. Circuits, Syst. Comput.*, vol. 27, no. 11, Oct. 2018, Art. no. 1850170, doi: 10.1142/S0218126618501700.

[22] A. Kartci, A. Agambayev, M. Farhat, N. Herencsar, L. Brancik, H. Bagci, and K. N. Salama, "Synthesis and optimization of fractional-order elements using a genetic algorithm," *IEEE Access*, vol. 7, pp. 80233–80246, 2019, doi: 10.1109/ACCESS.2019.2923166.

[23] S. Kapoulea, C. Psychalinos, A. S. Elwakil, and A. G. Radwan, "One-terminal electronically controlled fractional-order capacitor and inductor emulator," *AEU Int. J. Electron. Commun.*, vol. 103, pp. 32–45, May 2019, doi: 10.1016/j.aeue.2019.03.002.

[24] A. Adhikary, A. Shil, and K. Biswas, "Realization of foster structure-based ladder fractor with phase band specification," *Circuits, Syst., Signal Process.*, vol. 39, no. 5, pp. 2272–2292, May 2020, doi: 10.1007/s00034-019-01269-w.

[25] A. Charef, H. H. Sun, Y. Y. Tsao, and B. Onaral, "Fractal system as represented by singularity function," *IEEE Trans. Autom. Control*, vol. 37, no. 9, pp. 1465–1470, Sep. 1992, doi: 10.1109/9.159595.

[26] K. Matsuda and H. Fujii, "H_∞ optimized wave-absorbing control–analytical and experimental results," *J. Guid., Control, Dyn.*, vol. 16, no. 6, pp. 1146–1153, Nov. 1993, doi: 10.2514/3.21139.

[27] A. Oustaloup, F. Levron, B. Mathieu, and F. M. Nanot, "Frequency-band complex noninteger differentiator: Characterization and synthesis," *IEEE Trans. Circuits Syst. I, Fundam. Theory Appl.*, vol. 47, no. 1, pp. 25–39, Jan. 2000, doi: 10.1109/81.817385.

[28] R. El-Khazali, "On the biquadratic approximation of fractional-order Laplacian operators," *Anal. Integr. Circuits Signal Process.*, vol. 82, no. 3, pp. 503–517, Mar. 2015, doi: 10.1007/s10470-014-0432-8.

[29] A. M. AbdelAty, A. S. Elwakil, A. G. Radwan, C. Psychalinos, and B. J. Maundy, "Approximation of the fractional-order Laplacian s^α as a weighted sum of first-order high-pass filters," *IEEE Trans. Circuits Syst. II, Exp. Briefs*, vol. 65, no. 8, pp. 1114–1118, Aug. 2018, doi: 10.1109/TCSII.2018.2808949.

[30] S. Mahata, S. Saha, R. Kar, and D. Mandal, "Optimal integer-order rational approximation of α and $\alpha + \beta$ fractional-order generalised analogue filters," *IET Signal Process.*, vol. 13, no. 5, pp. 516–527, Mar. 2019, doi: 10.1049/iet-spr.2018.5340.

[31] S. Mahata, R. Kar, and D. Mandal, "Optimal approximation of fractional-order systems with model validation using CFOA," *IET Signal Process.*, vol. 13, no. 9, pp. 787–797, Dec. 2019, doi: 10.1049/iet-spr.2019.0158.

[32] A. Acharya, S. Das, I. Pan, and S. Das, "Extending the concept of analog Butterworth filter for fractional order systems," *Signal Process.*, vol. 94, pp. 409–420, Jan. 2014, doi: 10.1016/j.sigpro.2013.07.012.

[33] T. J. Freeborn, "Comparison of $(1 + \alpha)$ fractional-order transfer functions to approximate lowpass Butterworth magnitude responses," *Circuits, Syst., Signal Process.*, vol. 35, no. 6, pp. 1983–2002, Jun. 2016, doi: 10.1007/s00034-015-0226-y.

[34] N. Singh, U. Mehta, K. Kothari, and M. Cirrincione, "Optimized fractional low and highpass filters of $(1 + \alpha)$ order on FPAA," *Bull. Polish Acad. Sci. Tech. Sci.*, vol. 68, no. 3, pp. 635–644, 2020, doi: 10.24425/bpasts.2020.133123.

[35] A. Soni, N. Sreejeth, V. Saxena, and M. Gupta, "Series optimized fractional order low pass Butterworth filter," *Arabian J. Sci. Eng.*, vol. 45, no. 3, pp. 1733–1747, Mar. 2020, doi: 10.1007/s13369-019-04225-7.

[36] D. Kubanek, T. Freeborn, J. Koton, and N. Herencsar, "Evaluation of $(1 + \alpha)$ fractional-order approximated Butterworth high-pass and band-pass filter transfer functions," *Elektronika Elektrotechnika*, vol. 24, no. 2, pp. 37–41, Apr. 2018, doi: 10.5755/j01.eie.24.2.20634.

[37] S. Mahata, R. Kar, and D. Mandal, "Optimal fractional-order highpass Butterworth magnitude characteristics realization using current-mode filter," *AEU Int. J. Electron. Commun.*, vol. 102, pp. 78–89, Apr. 2019, doi: 10.1016/j.aeue.2019.02.014.

[38] T. J. B. Freeborn, B. Maundy, and A. S. Elwakil, "Field programmable analogue array implementation of fractional step filters," *IET Circuits Devices Syst.*, vol. 4, no. 6, pp. 514–524, Nov. 2010, doi: 10.1049/iet-cds.2010.0141.

[39] B. Maundy, A. S. Elwakil, and T. J. Freeborn, "On the practical realization of higher-order filters with fractional stepping," *Signal Process.*, vol. 91, no. 3, pp. 484–491, Mar. 2011, doi: 10.1016/j.sigpro.2010.06.018.

[40] C. Psychalinos, G. Tsirimokou, and A. S. Elwakil, "Switched-capacitor fractional-step Butterworth filter design," *Circuits, Syst., Signal Process.*, vol. 35, no. 4, pp. 1377–1393, Apr. 2016, doi: 10.1007/s00034-015-0110-9.

[41] S. Mahata, R. Kar, and D. Mandal, "Optimal modelling of $(1 + \alpha)$ order Butterworth filter under the CFE framework," *Fractal Fractional*, vol. 4, no. 4, p. 55, 2020, doi: 10.3390/fractalfract4040055.

[42] S. Mahata, S. K. Saha, R. Kar, and D. Mandal, "Optimal design of fractional order low pass Butterworth filter with accurate magnitude response," *Digit. Signal Process.*, vol. 72, pp. 96–114, Jan. 2018, doi: 10.1016/j.dsp.2017.10.001.

[43] S. Mahata, S. Banerjee, R. Kar, and D. Mandal, "Revisiting the use of squared magnitude function for the optimal approximation of $(1+\alpha)$-order Butterworth filter," *AEU Int. J. Electron. Commun.*, vol. 110, Oct. 2019, Art. no. 152826, doi: 10.1016/j.aeue.2019.152826.

[44] S. Mahata, R. Kar, and D. Mandal, "Comparative study of nature-inspired algorithms to design $(1 + \alpha)$ and $(2 + \alpha)$-order filters using a frequency-domain approach," *Swarm Evol. Comput.*, vol. 55, Jun. 2020, Art. no. 100685, doi: 10.1016/j.swevo.2020.100685.

[45] S. Mahata, R. Kar, and D. Mandal, "Optimal rational approximation of bandpass Butterworth filter with symmetric fractional-order roll-off," *AEU Int. J. Electron. Commun.*, vol. 117, Apr. 2020, Art. no. 153106, doi: 10.1016/j.aeue.2020.153106.

[46] S. Mahata, R. Kar, and D. Mandal, "Optimal approximation of asymmetric type fractional-order bandpass Butterworth filter using decomposition technique," *Int. J. Circuit Theory Appl.*, vol. 48, no. 9, pp. 1554–1560, Sep. 2020, doi: 10.1002/cta.2835.

[47] K. Ogata, *Modern Control Engineering*, 5th ed. New Delhi, India: Pearson, 2009.

[48] R. Verma, N. Pandey, and R. Pandey, "CFOA based low pass and high pass fractional step filter realizations," *AEU Int. J. Electron. Commun.*, vol. 99, pp. 161–176, Feb. 2019, doi: 10.1016/j.aeue.2018.11.032.

[49] E. M. Hamed, L. A. Said, A. H. Madian, and A. G. Radwan, "On the approximations of CFOA-based fractional-order inverse filters," *Circuits, Syst., Signal Process.*, vol. 39, no. 1, pp. 2–29, Jan. 2020, doi: 10.1007/s00034-019-01155-5.

SHIBENDU MAHATA received the M.Tech. degree in instrumentation and electronics engineering from Jadavpur University, India, in 2010. He was a Field Operations and Panel Engineer with Reliance Industries Ltd., and a Research Assistant with the Department of Cybernetics with CSIR-CMERI. He has authored above 40 articles published in SCI-E peer-reviewed journals, conference proceedings, and book chapters. His research interest includes optimal modeling of fractional-order filters. He was awarded with the University Medal for his M.Tech. from Jadavpur University. He was a recipient of the 2019 Premium Award for Best Paper from IET Signal Processing and the Best Paper Award from the 2016 IEEE International Conference on Computational Intelligence and Computing Research (ICCICR), Chennai, India.

NORBERT HERENCSAR (Senior Member, IEEE) received the Ph.D. degree from the Brno University of Technology (BUT), Czech Republic, in 2010. From 2013 to 2014, he was a Visiting Researcher with the Boğaziçi University, Turkey, and Doğuş University, Turkey. In 2019, he was a Visiting Professor with the University of Calgary, Canada, for six months. Since 2015, he has been an Associate Professor with the Department of Telecommunications, BUT. Since 2006, he has been collaborating on numerous research projects supported by the Czech Science Foundation. He is currently the Science Communications Manager and an MC Member of the COST Action CA15225 "Fractional-Order Systems-Analysis, Synthesis and Their Importance for Future Design." He has authored 101 articles published in SCI-E peer-reviewed journals and 122 papers in conference proceedings. His research interests include analog electronics, bioimpedance modeling, energy storage elements, fractional-order circuits and systems, impedance spectroscopy, instrumentation and measurement, sensory processing circuits and systems, and VLSI analog integrated circuits. Since 2013, he was an Organizing or a TPC Member of the AFRICON, ELECO, I^2MTC, ICUMT, IWSSIP, SET-CAS, MWSCAS, and ICECS conferences. He is a Senior Member of IACSIT and IRED, and a member of IAENG, ACEEE, and RS. In 2008–2016 and 2017–2020, he has been respectively an Organizing Committee Member and the General Co-Chair of the International Conference on Telecommunications and Signal Processing (TSP). Since 2021, he has been the General Chair of TSP. Since 2015, he has been serving in the IEEE Czechoslovakia Section Executive Committee as an SP/CAS/COM Joint Chapter Chair. Since 2011, he has been contributing as a Guest Co-Editor to several special journal issues in *AEÜ-International Journal of Electronics and Communications*, *Applied Sciences*, *Radioengineering*, *Telecommunication Systems*, and *Sensors*. Since 2014, he has been serving as an Associate Editor for IEEE Access, *Journal of Circuits, Systems and Computers*, and *IEICE Electronics Express (ELEX)*, and an Editorial Board Member of the *Radioengineering*, *Elektronika ir Elektrotechnika*, and *Fractal and Fractional*.

DAVID KUBANEK received the M.S. degree in electronics and communication and the Ph.D. degree in teleinformatics from the Brno University of Technology (BUT), Czech Republic, in 2002 and 2006, respectively. Since 2006, he has been an Assistant Professor with the Department of Telecommunications, BUT. He has authored 24 articles published in SCI-E peer-reviewed journals and about 35 papers in conference proceedings. He has participated on numerous research projects supported by the Czech Science Foundation. His research interests include design and analysis of analog electronic circuits, devices and elements, frequency filters, oscillators, impedance converters, non-linear circuits, and fractional-order circuits and systems. Since 2019, he has been serving as an Editorial Board Member of the *Fractal and Fractional* journal.